THERMAL STRESSES OF COMPOSITE BEAMS WITH RECTANGULAR

AND TUBULAR CROSS-SECTIONS

The members of the Committee approve the master's
thesis of Chia-Wei Su

Wen S. Chan
Supervising Professor

Haiying Huang

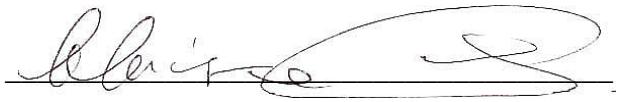

Kent L. Lawrence

THERMAL STRESSES OF COMPOSITE BEAMS WITH RECTANGULAR AND TUBULAR CROSS-SECTIONS

by

CHIA-WEI SU

Presented to the Faculty of the Graduate School of

The University of Texas at Arlington in Partial Fulfillment

of the Requirements

for the Degree of

MASTER OF SCIENCE IN MECHANICAL ENGINEERING

THE UNIVERSITY OF TEXAS AT ARLINGTON

December 2007

To my dear father, mother, sisters, and my lovely wife and daughter

for their endless support throughout my life

ACKNOWLEDGEMENTS

I would like to express my sincere appreciation and gratitude to my supervising professor, Dr. Wen S. Chan for his guidance and patience throughout my master's program and research. This thesis would not have been completed without his unlimited support and encouragement. I would also like to thank Dr. Kent L. Lawrence and Dr. Haiying Huang for serving as members of my committee.

Finally, I would to thank my father and sisters for their never ending support and encouragement from my home country, and also my wife and lovely daughter, Kathryn, for their understanding, patience and encouragement, which made this thesis possible.

November 12, 2007

ABSTRACT

THERMAL STRESSES OF COMPOSITE BEAMS WITH RECTANGULAR AND TUBULAR CROSS-SECTIONS

Publication No. _____

Chia-Wei Su, M.S.

The University of Texas at Arlington, 2007

Supervising Professor: Wen S. Chan

Closed-form analytical solutions for laminated composite beams with tubular and rectangular cross-sections are developed for evaluating the thermal induced stresses. The derivations are based on modified lamination theory and parallel axis theorem. The present approach includes variation of ply stiffness along the contour of the cross-section. The interlaminar shear stress of cantilever composite beam with rectangular cross-section under a transverse load is analytically proved to be independent of temperature change in uniform temperature environment. Three-dimensional finite element models for computing thermal stresses of both cross-sections are developed using commercial software package ANSYS 10. The results obtained from analytical solutions give an excellent agreement to finite element results.

The effects of stacking sequence and fiber orientation on the in-plane thermal stresses of laminate are studied by using present methods. It is found that fiber orientation plays a significant role on the thermal induced stresses between and within laminas.

TABLE OF CONTENTS

LIST OF ILLUSTRATIONS

LIST OF TABLES

CHAPTER 1

INTRODUCTION

1.1 Background

The fiber-reinforced composite material has been widely used in aerospace and military industrials for almost half century, due to its high specific stiffness and strength, good corrosion resistance, low density, and low coefficients of hygrothermal expansion. Initially, it was just applied to the secondary structures. With extensive researches and developments, composite materials have turned into the primary constituents of the major structures, such as fuselage and wings, of many aircrafts. Furthermore, during the past decade, it has also been put into everyday-used applications such as civil structures, sporting and recreational equipments, and automotive parts.

Among numerous applications of fiber reinforced composite materials, thin walled structures, such as circular tube and rectangular tube, are the most commonly used ones, due to their high stiffness/strength-weight ratio. Tubular structure with circular cross-section is ideally used as the basis for many applications since it has symmetrical geometry without edges. As a result, stresses at the free edge are eliminated. The legendary automaker Automobili Lamborghini SpA designed an engine subframe constructed by carbon/epoxy tubes and joints instead of steel subframe using on their new open-cockpit supercar, Murcielago Roadster. This design not only

successfully added back the loosing torsion stiffness caused by removal of its steel roof, but also reduced 17.7 lb of weight compare to using steel subframe.

Furthermore, the structure members are often exposed to the environments with temperature change during their service life. It has already been known that the thermal behaviors of the laminated composite materials are more pronounced than that of isotropic materials. Moreover, thermal stresses induced within and between laminas even without any global constraint. This is because of the thermal expansion mismatch between layers of different fiber orientations.

Due to its anisotropic material properties, the design of composite structures is quite complicated, and expensive tools are needed. Finite element analysis is one of the approaches that are often used in the analysis of laminated composite structures, and able to make accurate prediction of structural behaviors. However, it is still not an efficient and handy method since the analysis is structural configuration dependant and time consuming. Furthermore, the finite element analysis of composite structures is not a cost effective way to conduct the parametric study during design practice. Hence, in order to effectively design composite structure, simple but yet sufficiently accurate analytical models are needed to be developed, particularly in the preliminary design stage.

1.2 Literature Survey

In the past decades, considerable of good researches in laminated composite beam structures have been published. Extensive have been made to understand the

structural behaviors, such as bending stiffness, of the laminated composite thin-wall structure under various load condition. Several different analytical models have been developed to obtain simple close-form solutions for laminated composite structures. Among them, equivalent stiffness of the wall laminate of the thin-walled structures has been used.

Chan and Demirhan [1] have developed two analytical closed-form solutions, laminated plate approach and laminated shell approach, to evaluate stiffness matrices and bending stiffness of the laminated composite circular tube. The derivations are based on conventional lamination theory and parallel axis theory. Analytical results are compared with the results obtained from the smear property approach and finite element analysis. Lin and Chan [2] extended the former tube model to analyze laminated composite tubes with elliptical cross-section under bending. The obtained analytical results show an excellent agreement with finite element method results. Rao [3] has developed closed-form expressions based on modifying the laminated plate approach to determine the displacement and twisting angle of tapered composite tube under axial tension and torsion.

Sims and Wilson [4] have derived an approximate elasticity solution for the transverse shearing stresses in a multilayered anisotropic composite beam. The distribution of shear stresses through the laminate thickness obtained from analytical solution has been validated by experimental data. Syed and Chan [5] have developed an analytical model to analyze the bending stiffness matrices for laminated composite beam with hat cross-section. The thermal induced ply stresses and the location of

centroid and shear center of the hat sectional composite beam have also been included in his study.

Other researches have been focused on induced stresses between and within laminas while laminated composite structures are subjected to temperature change. Boley and Weiner [6] describe the general theory of thermal stresses of beam structures in their published book.

Using finite element method to analyze the behavior of laminated composite structure under temperature environment is one of the common approaches. Naidu and Sinha [7] have studied the large deflection and bending behavior of composite cylindrical shell panels subjected to hygrothermal environment using nonlinear finite element analysis. Seibi and Amatcau [8] have researched on the use of the laminated plate theory (LPT) to optimize the architecture of laminated ceramic matrix composite tube processing high thermal cracking resistance. They have developed a method to estimate the induced thermal residual stresses of laminated composite tube under significant temperature change using finite element modeling program ANSYS. Shariyat [9] has studied for thermal buckling analysis of rectangular composite multilayered plate under uniform temperature rise using a layerwise plate theory to determine the buckling temperature.

However, finite element analysis is still not an efficient method because of structural configuration dependent. Hence, some other efforts have been made on developing analytical models and close-form expressions for thermal analysis of composite laminates. Kim, B., Kim, T., Byun, and Lee [10] have derived a close-form

solution for composite/ceramic tube to calculate the shrink fit stresses, the stresses due to internal pressure and thermal stresses due to temperature differences between the inside and outside of the tube. Khdeir [11] has developed an exact analytical solution of refined beam theories to obtain the critical buckling temperature of cross-ply beam subjected to uniform temperature distribtion with various boundary conditions. Additionally, Syed, Su, and Chan [12] have presented simple analytical expressions for computing thermal stresses in fiber reinforced composite beam with rectangular and hat cross-sections under uniform temperature environment. In-plane stresses and interlaminar shear stress were also analyzed.

For designing composite beam structure, the developing of analytical method not only provide accurate evaluation of sectional properties for better prediction of structure behaviors, but also can be much easier used for parametric study.

1.3 Objective and Approach of the Thesis

In the present research, the primary objective is to develop closed-form solutions for laminated composite circular tube, and rectangular beam to determine their thermal induced load and moment matrices, based on lamination theory, parallel axis theory, and laminated plate approach [1]. In-plane stresses and interlaminar shear stress through the thickness of the laminate are also studied. Results are compared and validated by performing finite element analysis of fully three-dimensional constructed models. The finite element models are developed in the commercial software package ANSYS 10, and verified by first applying properties of isotropic material on them. In

this study, the composite material Carbon/Epoxy AS4/3501-6 is chosen for both cases. Further, the parametric studies are conducted to study the stacking sequence and fiber orientation effects on the thermal induced in-plane stresses.

1.4 Outline of the Thesis

In Chapter 2, the analytical solution for rectangular composite beam is derived, and the lamination theory is reviewed. The analytical solution for composite circular tube and the review of stiffness matrices based on laminated plate approach are described in Chapter 3. Chapter 4 describes two three-dimensional finite element models used to validate analytical approach. Further, comparisons between the results obtained from analytical solutions and finite element models are listed in Chapter 5. Parametric studies are also included in this chapter. Finally, the conclusions are summarized in Chapter 6. The details of derivations, MATLAB codes, and ANSYS batch files are presented in Appendix section.

CHAPTER 2

ANALYTICAL SOLUTION FOR RECTANGULAR COMPOSITE BEAM UNDER TEMPERATURE ENVIRONMENT

In this chapter, an analytical method for thermal analysis of a rectangular composite beam is presented. Since all the derivations are based on conventional lamination theory, it is also briefly reviewed. The geometry of the rectangular composite beam is first defined in the next section.

2.1 Geometry of Composite Beam

The composite beam studied here is a rectangular cross-section beam with the width, d and the height, h. The length, L of the composite beam is significantly longer than its width and height. In all the derivations, the cross-sectional plane of the beam remaining plane after deformation is assumed.

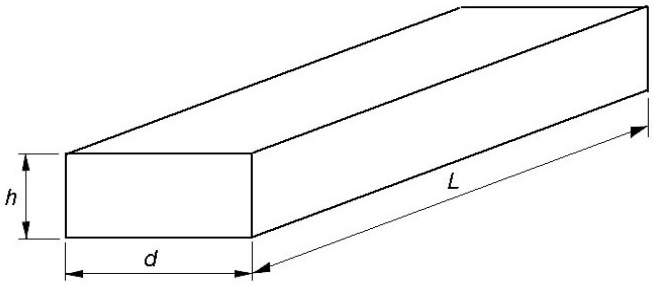

Fig. 2.1 Geometry of composite beam

2.2 Review of Laminated Constitutive Equation

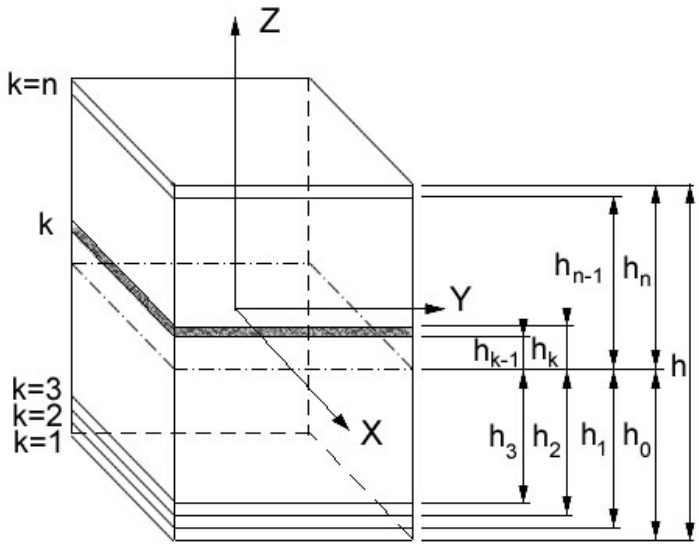

Fig. 2.2 Composite laminate with n layers

Composite laminate consists of a set of multiple layers with different fiber orientations stacking together as shown in Fig. 2.2. When laminate is subjected to load, each layer exhibits different stresses. It is very cumbersome to analyze this problem based on layer by layer analysis. To circumvent this tedious approach, the laminate is often analyzed based upon its mid-plane axes as a reference axis. In doing so, the properties of each layer are transformed to the reference axis.

The general load-deformation relation of laminate is given as:

$$\begin{bmatrix} \overline{N} \\ \overline{M} \end{bmatrix} = \begin{bmatrix} A & \mathrm{B} \\ \mathrm{B} & \mathrm{D} \end{bmatrix} \cdot \begin{bmatrix} \varepsilon^0 \\ \kappa \end{bmatrix} \tag{2.1}$$

Where $[\varepsilon^0]$ and $[\kappa]$ matrices are mid-plane strain and curvature, respectively. $[\overline{N}]$ and $[\overline{M}]$ are given as:

$$\begin{bmatrix} \overline{N} \\ \overline{M} \end{bmatrix} = \begin{bmatrix} \mathrm{N} \\ \mathrm{M} \end{bmatrix} + \begin{bmatrix} N^T \\ M^T \end{bmatrix} \tag{2.2}$$

$[N]$ and $[M]$ are the equivalent applied load and moment, respectively. They can be written as:

$$\begin{aligned} [N] &= \sum_{k=1}^{n} \int_{z_{k-1}}^{z_k} [\sigma]_k \cdot dz \\ [M] &= \sum_{k=1}^{n} \int_{z_{k-1}}^{z_k} [\sigma]_k \cdot z \cdot dz \end{aligned} \tag{2.3}$$

$[N^T]$ and $[M^T]$ are the thermal induced force and moment which are given as:

$$[N^T] = \left\{ \sum_{k=1}^{n} [\overline{Q}]_k \cdot [\alpha_{x-y}]_k \cdot (h_k - h_{k-1}) \right\} \cdot \Delta T \tag{2.4}$$

$$[M^T] = \frac{1}{2} \left\{ \sum_{k=1}^{n} [\overline{Q}]_k \cdot [\alpha_{x-y}]_k \cdot ({h_k}^2 - {h_{k-1}}^2) \right\} \cdot \Delta T \tag{2.5}$$

In the above equations, $[\alpha_{x-y}]_k$ is the coefficient of thermal expansion, CTE, of k^{th} ply transforming from material 1-2 coordinate system to the laminate x-y coordinate system. ΔT is the change of environmental temperature. h_k is the

coordinate of the top of k^{th} ply (see Fig. 2.2). The transformation of CTE, $[\alpha_{x-y}]_k$, is given in the Appendix.

Furthermore, $[A]$, $[B]$, and $[D]$ matrices in equation 2.1 are the extensional stiffness, extensional-bending coupling stiffness, and bending stiffness, respectively. They are the properties evaluated per unit width of the laminate, and can be expressed as:

$$[A] = \sum_{k=1}^{n} [\overline{Q}]_k \cdot (h_k - h_{k-1})$$

$$[B] = \frac{1}{2} \sum_{k=1}^{n} [\overline{Q}]_k \cdot (h_k^{\,2} - h_{k-1}^{\,2}) \tag{2.6}$$

$$[D] = \frac{1}{3} \sum_{k=1}^{n} [\overline{Q}]_k \cdot (h_k^{\,3} - h_{k-1}^{\,3})$$

Where $[\overline{Q}]_k$ is obtained from the transformation of the reduced stiffness matrix, $[Q]$ of the laminate. z_k refers to the z coordinate of k^{th} interface measured from the mid-plane of the laminate. The reduced stiffness matrix, $[Q]$ is the stiffness of thin layer of orthotropic material. $[Q]$ matrix represents the relationship of stress and strain in its material coordinate system, which can be written as:

$$\begin{bmatrix} \sigma_1 \\ \sigma_2 \\ \tau_{12} \end{bmatrix} = \begin{bmatrix} Q_{11} & Q_{12} & 0 \\ Q_{21} & Q_{22} & 0 \\ 0 & 0 & Q_{66} \end{bmatrix} \cdot \begin{bmatrix} \varepsilon_1 \\ \varepsilon_2 \\ \gamma_{12} \end{bmatrix} \tag{2.7}$$

and $[Q]$ matrix is defined as:

$$\begin{aligned} Q_{11} &= \frac{E_1}{1-\nu_{12}\nu_{21}} \\ Q_{22} &= \frac{E_2}{1-\nu_{12}\nu_{21}} \\ Q_{21} &= Q_{12} = \frac{\nu_{21}E_1}{1-\nu_{12}\nu_{21}} = \frac{\nu_{12}E_1}{1-\nu_{12}\nu_{21}} \\ Q_{66} &= G_{12} \end{aligned} \tag{2.8}$$

Where E_1 and E_2 are the elastic moduli of lamina along and transverse to the fiber direction, respectively. G_{12} is the shear modulus lamina in 1-2 plane, and ν_{12} is the poisson's ratio of lamina for the loading along the fiber direction.

2.3 In-Plane Stresses

The total strain at any point in the k^{th} ply of the laminate can be obtained from the mid-plane strain, $[\varepsilon^0]$, the curvature, $[\kappa]$, and the coordinate in z direction measured from the mid-plane. It can be determined using the following relationship:

$$\begin{bmatrix} \varepsilon_x \\ \varepsilon_y \\ \gamma_{xy} \end{bmatrix}_k = \begin{bmatrix} \varepsilon_x^0 \\ \varepsilon_y^0 \\ \gamma_{xy}^0 \end{bmatrix} + z \cdot \begin{bmatrix} \kappa_x \\ \kappa_y \\ \kappa_{xy} \end{bmatrix} \tag{2.9}$$

Note that the strain obtained from the equation above is the total strain contributed by both mechanical loads and thermal expansion. Hence, the strain due to thermal expansion needs to be subtracted from the total strain in the calculation of the in-plane stresses, which can be expressed as below:

$$[\varepsilon_{x-y}]_k = [\varepsilon_{x-y}]_k - [\varepsilon^T_{x-y}]_k$$

$$= [\varepsilon_{x-y}]_k - [\alpha_{x-y}]_k \cdot \Delta T \tag{2.10}$$

$$[\sigma_{x-y}]_k = [\overline{Q}]_k \cdot \left\{ [\varepsilon_{x-y}]_k - [\alpha_{x-y}]_k \cdot \Delta T \right\}$$

$$= [\overline{Q}]_k \cdot \left\{ [\varepsilon^0] + z \cdot [\kappa] - [\alpha_{x-y}]_k \cdot \Delta T \right\} \tag{2.11}$$

Where $[\varepsilon_{x-y}]_k$ and $[\varepsilon^T_{x-y}]_k$ represent strain of the k^{th} ply of the laminate due to mechanical loads and thermal expansion, respectively.

2.4 Interlaminar Shear Stress of the Beam under Transverse Load

In this section, an analytical solution for the interlaminar shear stresses of the laminated composite beam subjected to a transverse load developed by Sims and Wilson [4] is first reviewed. The effect due to thermal induced force and moment in the interlaminar shear stresses is then discussed. In the derivation of the analytical solution, two assumptions are made: 1. the stresses do not depend on y direction. 2. σ_z, τ_{yz} are small and can be neglected. The geometry of the beam model and coordinate axes are shown in Fig. 2.3.

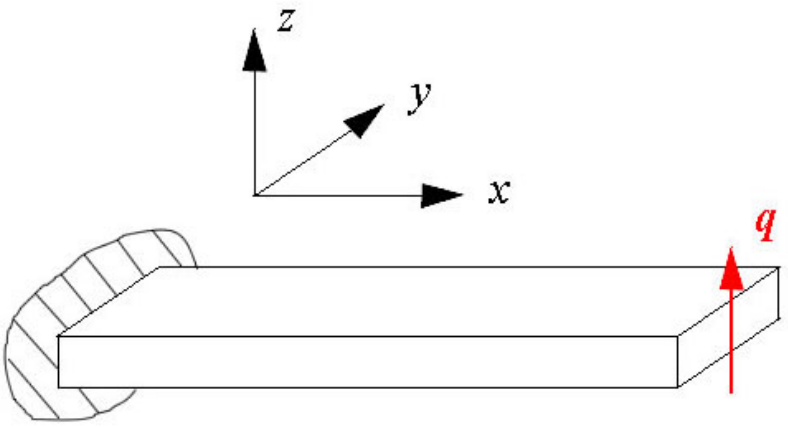

Fig. 2.3 Laminated composite beam under transverse load.

2.4.1 Derivation of Interlaminar Shear Stress Equation

The equation of equilibrium for the k^{th} layer of the laminate is given as:

$$\frac{\partial \sigma_x^k}{\partial x}+\frac{\partial \tau_{xy}^k}{\partial y}+\frac{\partial \tau_{xz}^k}{\partial z}=0$$

$$\frac{\partial \tau_{xy}^k}{\partial x}+\frac{\partial \sigma_y^k}{\partial y}+\frac{\partial \tau_{yz}^k}{\partial z}=0 \qquad (2.12)$$

$$\frac{\partial \tau_{xz}^k}{\partial x}+\frac{\partial \tau_{yz}^k}{\partial y}+\frac{\partial \sigma_z^k}{\partial z}=0$$

It is known that in the conventional lamination theory, the lamina is assumed to be under plane stress condition. That means, the stresses σ_z, τ_{yz}, and τ_{xz} are assumed to be zero. Therefore, interlaminar stress components will not be obtained directly from the lamination theory. However, these stresses can only be obtained from equation of equilibrium as shown in equation 2.12. Since the free edge stresses is not the focus of this study, the rise of σ_z, τ_{yz}, and τ_{xz} due to the free edge is ignored. In addition, since

the beam is narrow, the stresses are assumed to be independent of y. Then, equation 2.12 can be reduced to:

$$\frac{\partial \sigma_x^k}{\partial x} + \frac{\partial \tau_{xz}^k}{\partial z} = 0 \tag{2.13}$$

Thus,

$$\tau_{xz}^k = -\int_{z_{k-1}}^{z_k} \frac{\partial \sigma_x^k}{\partial x} \cdot dz + \tau_{xz}^{k-1} \tag{2.14}$$

For multiple layers laminate with $\tau_{xz}^0 = 0$, we have

$$\tau_{xz}^k = -\sum_{i=1}^{k} \int_{z_{i-1}}^{z_i} \frac{\partial \sigma_x^i}{\partial x} \cdot dz \tag{2.15}$$

Based on the conventional lamination theory, the laminated constitutive equation including thermal effect is given as:

$$\begin{bmatrix} \varepsilon^0 \\ \kappa \end{bmatrix} = \begin{bmatrix} a & \mathrm{b} \\ \mathrm{b}^{\mathrm{T}} & \mathrm{d} \end{bmatrix} \cdot \begin{bmatrix} N + N^T \\ M + M^T \end{bmatrix} \tag{2.16}$$

Where,

$$\begin{bmatrix} a & \mathrm{b} \\ \mathrm{b}^{\mathrm{T}} & \mathrm{d} \end{bmatrix} = \begin{bmatrix} A & B \\ B & D \end{bmatrix}^{-1} \tag{2.17}$$

Since the cantilevered rectangular beam is under a transverse shear load, q, the in-plane forces are not considered on the beam. Furthermore, in this derivation, the cantilever beam is considered as a narrow beam. Hence, we have:

$$N_x = N_y = N_{xy} = M_y = M_{xy} = 0$$

and,

$$\frac{\partial M_x}{\partial x} = -q \tag{2.18}$$

Note that q is the transverse load per unit width. Then, equation 2.16 becomes:

$$\begin{aligned} [\varepsilon^0] &= [a]\cdot[N^T] + [b]\cdot[M + M^T] \\ [\kappa] &= [b^T]\cdot[N^T] + [d]\cdot[M + M^T] \end{aligned} \tag{2.19}$$

Substituting equation 2.11, 2.19 into equation 2.15, we get:

$$\begin{aligned} \tau_{xz}^k &= -\sum_{i=1}^{k} \int_{z_{i-1}}^{z_i} \frac{\partial \sigma_x^i}{\partial x}\cdot dz \\ &= -\sum_{i=1}^{k} \int_{z_{i-1}}^{z_i} \left\{ \overline{Q}_{11}^i \left(\frac{\partial \varepsilon_x^0}{\partial x} + z_i \cdot \frac{\partial \kappa_x}{\partial x}\right) + \overline{Q}_{12}^i \left(\frac{\partial \varepsilon_y^0}{\partial x} + z_i \cdot \frac{\partial \kappa_y}{\partial x}\right) \right. \\ &\qquad \left. + \overline{Q}_{16}^i \left(\frac{\partial \gamma_{xy}^0}{\partial x} + z_i \cdot \frac{\partial \kappa_{xy}}{\partial x}\right) \right\} \cdot dz \end{aligned} \tag{2.20}$$

Since $[N^T]$ and $[M^T]$ for this case do not depend on x, their partial derivatives are eliminated. Hence, equation 2.20 becomes:

$$\begin{aligned} \tau_{xz}^k &= -\sum_{i=1}^{k} \int_{z_{i-1}}^{z_i} \{\overline{Q}_{11}^i[(-b_{11}\cdot q) + z_i\cdot(-d_{11}\cdot q)] + \overline{Q}_{12}^i[(-b_{21}\cdot q) + z_i\cdot(-d_{21}\cdot q)] \\ &\qquad + \overline{Q}_{16}^i[(-b_{61}\cdot q) + z_i\cdot(-d_{61}\cdot q)]\}\cdot dz \\ &= \sum_{i=1}^{k} \int_{z_{i-1}}^{z_i} [(\overline{Q}_{11}^i b_{11} + \overline{Q}_{12}^i b_{21} + \overline{Q}_{16}^i b_{61}) + z_i\cdot(\overline{Q}_{11}^i d_{11} + \overline{Q}_{12}^i d_{21} + \overline{Q}_{16}^i d_{61})]\cdot q\cdot dz \\ &= \sum_{i=1}^{k} \int_{z_{i-1}}^{z_i} [QB_i + z_i\cdot QD_i]\cdot q\cdot dz \\ &= q\cdot\left\{\sum_{i=1}^{k} QB_i(z_i - z_{i-1}) + \frac{1}{2}\cdot\sum_{i=1}^{k} QD_i({z_i}^2 - {z_{i-1}}^2)\right\} \end{aligned} \tag{2.21}$$

It is noted that the above expression of τ_{xz} does not induce any properties that depends on temperature. Therefore, the thermal induced force and moment do not affect the result of interlaminar shear stresses of a laminated composite beam under transverse load.

CHAPTER 3

ANALYTICAL SOLUTION FOR COMPOSITE TUBULAR BEAM UNDER TEMPERATURE ENVIRONMENT

In this chapter, an analytical method for thermal analysis of a circular composite tube is presented. Additionally, an analytical solution of stiffness matrices of laminated composite tube developed by Chan and Demirhan [1] is reviewed. The parallel axis theorem used in the derivation is also described. Then, the geometry of the circular composite tube that is considered in this study is described in the next section.

3.1 Geometry of Composite Tube

The composite tube studied here is a hollow circular cross-section tube with inner radius, R_i , and outer radius, R_o . The length, L of the composite tube is significantly longer than its diameter. This minimizes the short tube effect. In all the derivations, the cross-sectional plane of the tube will always remain plane after deformation is assumed.

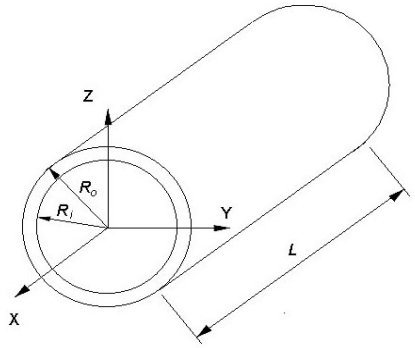

Fig. 3.1 Geometry of Composite Tube

3.2 Review of the Parallel Axis Theorem

In lamination theory, the reference axis is often set at the mid-plane of laminate. However, in structural modeling, the reference axis is not always in the mid-plane of the laminate. Hence, the stiffness matrices of the whole structure can be obtained by translating the stiffness of the laminate according to parallel axis theorem. The stiffness matrices referring to a new axis can be written as:

$$\begin{aligned} [A'] &= [A] \\ [B'] &= [B] + d \cdot [A] \\ [D'] &= [D] + 2d \cdot [B] + d^2 \cdot [A] \end{aligned} \tag{3.1}$$

where d is the distance from new axis to the original axis as shown in Fig 3.2.

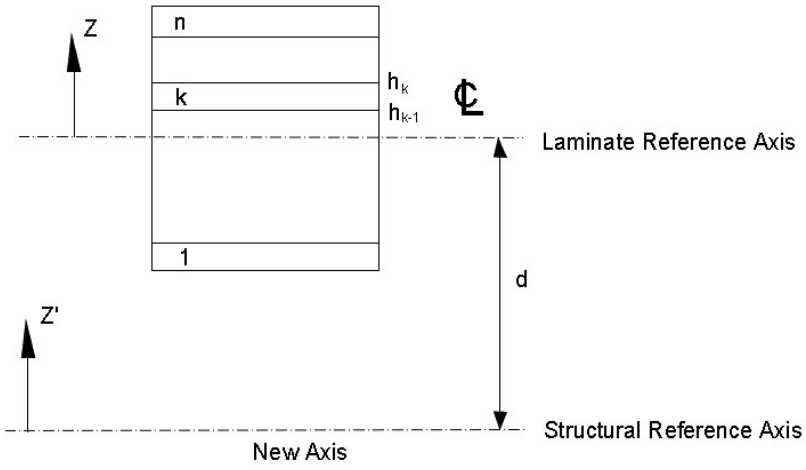

Fig. 3.2 Translation of laminate axis

3.3 Stiffness Matrices of Tubular Composite Beam

Two analytical methods, laminated plate approach and laminated shell approach, for evaluating stiffness matrices of circular composite tube were developed by Chan and Demirhan [1]. Plate approach is chosen here because of its simplicity. Both of these two approaches were derived based on the conventional lamination theory and translation of laminate axis.

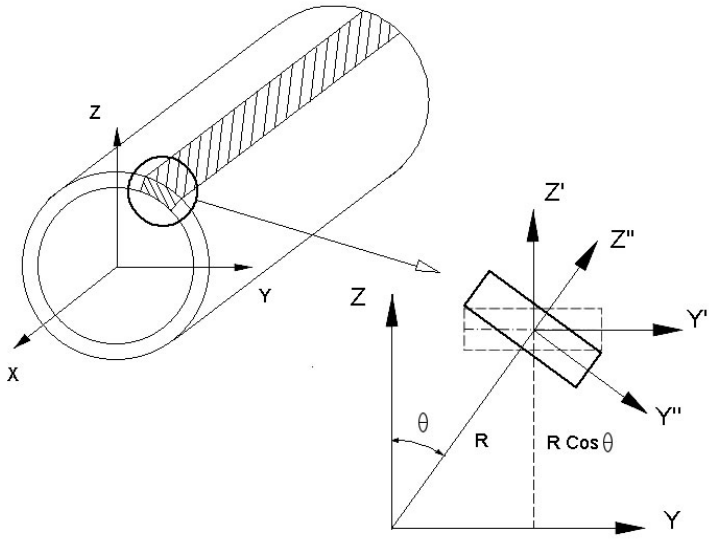

Fig. 3.3 Infinitesimal plate element of composite tube

In this approach, an infinitesimal plate element of laminated composite tube is considered. The infinitesimal element, which is inclined an angle, θ, with respect to the axis of the tube, z, is rotated about the x'' axis as shown in Fig. 3.3. Thus, the reduced stiffness matrix of lamina, $[Q]$ needs to be first transformed about x'' axis with an angle, θ, then transformed about z' axis with the angle of fiber orientation of the ply.

The transformed reduced stiffness matrix of k^{th} ply is represented as $[\hat{Q}]_k$. The transformation of the $[\hat{Q}]_k$ is given in Appendix A. Then, the stiffness matrices of the infinitesimal plate element of the composite tube become:

$$A_{ij} = \sum_{k=1}^{n} \hat{Q}_{ij}^{k} (z'_k - z'_{k-1})$$

$$B_{ij} = \sum_{k=1}^{n} \hat{Q}_{ij}^{k} (z'^{2}_k - z'^{2}_{k-1}) \tag{3.2}$$

$$D_{ij} = \sum_{k=1}^{n} \hat{Q}_{ij}^{k} (z'^{3}_k - z'^{3}_{k-1})$$

Base on the parallel axis theorem, the stiffness matrices of the infinitesimal plate element of the composite tube, $[A]$, $[B]$,and $[D]$, have to be translated to the reference axis of the tube. Hence, the stiffness matrices per unit width of the tube, $[A']$, $[B']$,and $[D']$, can be expressed as below:

$$\begin{aligned} [A'] &= [A] \\ [B'] &= [B] + R \cdot \cos\theta \cdot [A] \\ [D'] &= [D] + 2R \cdot \cos\theta \cdot [B] + (R \cdot \cos\theta)^2 \cdot [A] \end{aligned} \tag{3.3}$$

Then, the overall stiffness matrices of the circular composite tube are obtained by integrating the stiffness matrices per unit width of the tube, $[A']$, $[B']$, and $[D']$, over its entire length of the circumference. They are expressed as:

$$\left[\overline{A}\right] = \int_0^{2\pi} \left[A'\right] \cdot R \cdot d\theta$$

$$\left[\overline{B}\right] = \int_0^{2\pi} \left[B'\right] \cdot R \cdot d\theta \tag{3.4}$$

$$\left[\overline{D}\right] = \int_0^{2\pi} \left[D'\right] \cdot R \cdot d\theta$$

Fig. 3.4 illustrates the computing procedure for obtaining the stiffness matrix of composite tubular structures.

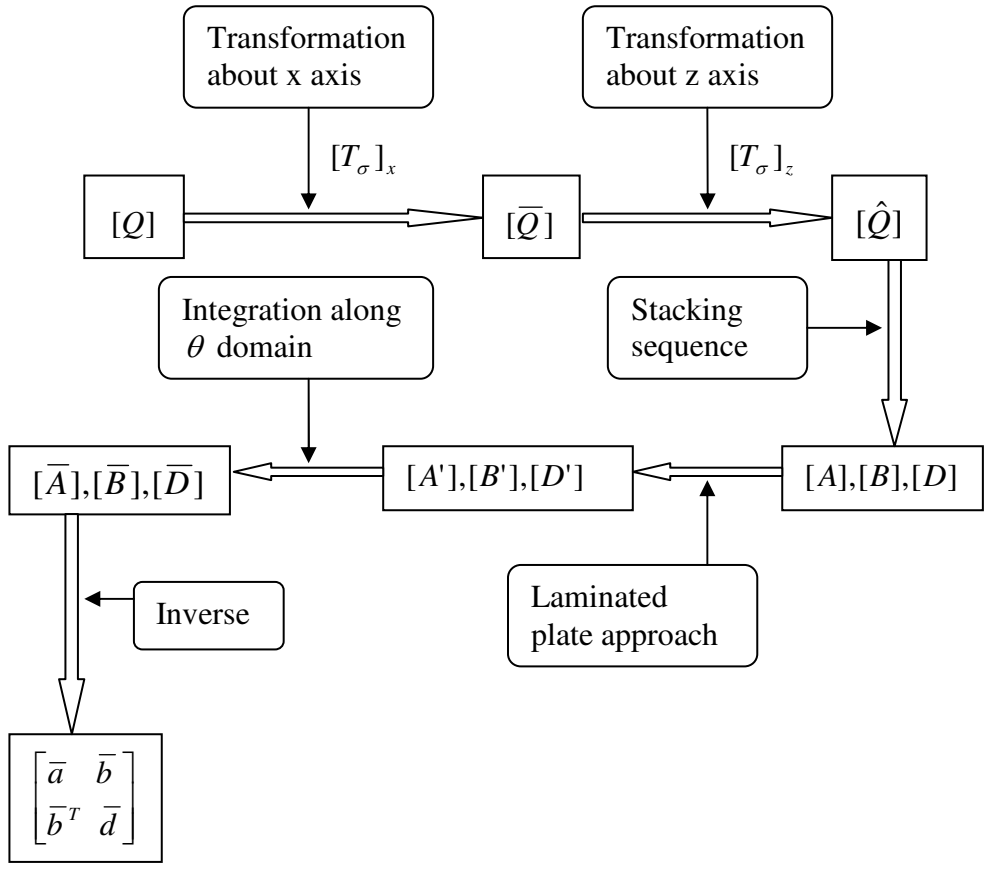

Fig. 3.4 Procedure flow chart for computing stiffness matrix

3.4 Thermal Induced Force and Moment

3.4.1 Transformation of the Coefficient of Thermal Expansion

The coefficient of thermal expansion of k^{th} ply of the composite beam in its structural x-y coordinate system, $[\alpha_{x-y}]_k$ is obtained from transforming the coefficient of thermal expansion of the lamina in 1-2 coordinate, $[\alpha_{1-2}]$. Referring to Fig. 3.3, it is first rotated about the x axis with an angle θ, then, rotated about z axis with the angle of fiber orientation, $-\beta$. The transformation of the thermal expansion coefficient can be written as:

$$[\alpha'_{1-2}] = [T_\varepsilon(\theta)] \cdot [\alpha_{1-2}]$$

$$[\alpha_{x-y}]_k = [T_\varepsilon(-\beta)]_k \cdot [\alpha'_{1-2}] \tag{3.5}$$

In the above equation, $[T_\varepsilon]$ matrices are the strain transformation matrices transforming about x and z axis, respectively. They are provided in Appendix A.

3.4.2 Unit Thermal Induced Force and Moment

Similar as deriving stiffness matrices with laminated plate approach, an infinitesimal plate element is considered as shown in Fig.3.3. The thermal induced force and moment of the element are obtained by integrating thermal strain through the thickness of lamina, and can be written as:

$$N_{x'}^{T} = \Delta T \cdot \sum_{k=1}^{n} (\hat{Q}_{11}^{k} \cdot \alpha_{x}^{k} + \hat{Q}_{12}^{k} \cdot \alpha_{y}^{k} + \hat{Q}_{16}^{k} \cdot \alpha_{xy}^{k}) \cdot (z_{k}^{'} - z_{k-1}^{'})$$

$$N_{y'}^{T} = \Delta T \cdot \sum_{k=1}^{n} (\hat{Q}_{12}^{k} \cdot \alpha_{x}^{k} + \hat{Q}_{22}^{k} \cdot \alpha_{y}^{k} + \hat{Q}_{26}^{k} \cdot \alpha_{xy}^{k}) \cdot (z_{k}^{'} - z_{k-1}^{'}) \tag{3.6}$$

$$N_{xy'}^{T} = \Delta T \cdot \sum_{k=1}^{n} (\hat{Q}_{16}^{k} \cdot \alpha_{x}^{k} + \hat{Q}_{26}^{k} \cdot \alpha_{y}^{k} + \hat{Q}_{66}^{k} \cdot \alpha_{xy}^{k}) \cdot (z_{k}^{'} - z_{k-1}^{'}),$$

and

$$M_{x'}^{T} = \frac{\Delta T}{2} \cdot \sum_{k=1}^{n} (\hat{Q}_{11}^{k} \cdot \alpha_{x}^{k} + \hat{Q}_{12}^{k} \cdot \alpha_{y}^{k} + \hat{Q}_{16}^{k} \cdot \alpha_{xy}^{k}) \cdot (z_{k}^{'2} - z_{k-1}^{'2})$$

$$M_{y'}^{T} = \frac{\Delta T}{2} \cdot \sum_{k=1}^{n} (\hat{Q}_{12}^{k} \cdot \alpha_{x}^{k} + \hat{Q}_{22}^{k} \cdot \alpha_{y}^{k} + \hat{Q}_{26}^{k} \cdot \alpha_{xy}^{k}) \cdot (z_{k}^{'2} - z_{k-1}^{'2}) \tag{3.7}$$

$$M_{xy'}^{T} = \frac{\Delta T}{2} \cdot \sum_{k=1}^{n} (\hat{Q}_{16}^{k} \cdot \alpha_{x}^{k} + \hat{Q}_{26}^{k} \cdot \alpha_{y}^{k} + \hat{Q}_{66}^{k} \cdot \alpha_{xy}^{k}) \cdot (z_{k}^{'2} - z_{k-1}^{'2}),$$

where $\hat{Q}_{ij}^{k}$ is the transformed reduced stiffness matrix, and ΔT is the change of the temperature.

3.4.3 Parallel Axis Theorem Applied to Transfer Thermal Induced Loads

The forces and moments obtained using equation 3.6 and 3.7 act along the mid plane of the lamina. In order to transfer these resultants to the reference axis of the tube structure, the parallel axis theorem is applied. In the present case, as shown in Fig.3.3, the distant from new reference axis to the original axis, d is equal to $R \cdot \cos\theta$. Then, the thermal induced force and moment per unit width of the tube become:

$$N_x^T = \Delta T \cdot \sum_{k=1}^{n} (\hat{Q}_{11}^k \cdot \alpha_x^k + \hat{Q}_{12}^k \cdot \alpha_y^k + \hat{Q}_{16}^k \cdot \alpha_{xy}^k) \cdot [(z_k^{'} + R \cdot \cos\theta) - (z_{k-1}^{'} + R \cdot \cos\theta)]$$
$$= \Delta T \cdot \sum_{k=1}^{n} (\hat{Q}_{11}^k \cdot \alpha_x^k + \hat{Q}_{12}^k \cdot \alpha_y^k + \hat{Q}_{16}^k \cdot \alpha_{xy}^k) \cdot (z_k^{'} - z_{k-1}^{'}) = N_{x'}^T$$

$$N_y^T = \Delta T \cdot \sum_{k=1}^{n} (\hat{Q}_{12}^k \cdot \alpha_x^k + \hat{Q}_{22}^k \cdot \alpha_y^k + \hat{Q}_{26}^k \cdot \alpha_{xy}^k) \cdot [(z_k^{'} + R \cdot \cos\theta) - (z_{k-1}^{'} + R \cdot \cos\theta)] \quad (3.8)$$
$$= \Delta T \cdot \sum_{k=1}^{n} (\hat{Q}_{12}^k \cdot \alpha_x^k + \hat{Q}_{22}^k \cdot \alpha_y^k + \hat{Q}_{26}^k \cdot \alpha_{xy}^k) \cdot (z_k^{'} - z_{k-1}^{'}) = N_{y'}^T$$

$$N_{xy}^T = \Delta T \cdot \sum_{k=1}^{n} (\hat{Q}_{16}^k \cdot \alpha_x^k + \hat{Q}_{26}^k \cdot \alpha_y^k + \hat{Q}_{66}^k \cdot \alpha_{xy}^k) \cdot [(z_k^{'} + R \cdot \cos\theta) - (z_{k-1}^{'} + R \cdot \cos\theta)]$$
$$= \Delta T \cdot \sum_{k=1}^{n} (\hat{Q}_{16}^k \cdot \alpha_x^k + \hat{Q}_{26}^k \cdot \alpha_y^k + \hat{Q}_{66}^k \cdot \alpha_{xy}^k) \cdot (z_k^{'} - z_{k-1}^{'}) = N_{xy'}^T$$

and

$$M_x^T = \frac{\Delta T}{2} \cdot \sum_{k=1}^{n} (\hat{Q}_{11}^k \cdot \alpha_x^k + \hat{Q}_{12}^k \cdot \alpha_y^k + \hat{Q}_{16}^k \cdot \alpha_{xy}^k) \cdot [(z_k^{'} + R \cdot \cos\theta)^2 - (z_{k-1}^{'} + R \cdot \cos\theta)^2]$$
$$= \frac{\Delta T}{2} \cdot \sum_{k=1}^{n} (\hat{Q}_{11}^k \cdot \alpha_x^k + \hat{Q}_{12}^k \cdot \alpha_y^k + \hat{Q}_{16}^k \cdot \alpha_{xy}^k) \cdot [(z_k^{'2} - z_{k-1}^{'2}) + 2 \cdot R\cos\theta \cdot (z_k^{'} - z_{k-1}^{'})]$$
$$= M_{x'}^T + R \cdot \cos\theta \cdot N_{x'}^T$$

$$M_y^T = \frac{\Delta T}{2} \cdot \sum_{k=1}^{n} (\hat{Q}_{12}^k \cdot \alpha_x^k + \hat{Q}_{22}^k \cdot \alpha_y^k + \hat{Q}_{26}^k \cdot \alpha_{xy}^k) \cdot [(z_k^{'} + R \cdot \cos\theta)^2 - (z_{k-1}^{'} + R \cdot \cos\theta)^2]$$
$$= \frac{\Delta T}{2} \cdot \sum_{k=1}^{n} (\hat{Q}_{12}^k \cdot \alpha_x^k + \hat{Q}_{22}^k \cdot \alpha_y^k + \hat{Q}_{26}^k \cdot \alpha_{xy}^k) \cdot [(z_k^{'2} - z_{k-1}^{'2}) + 2 \cdot R\cos\theta \cdot (z_k^{'} - z_{k-1}^{'})] \quad (3.9)$$
$$= M_{y'}^T + R \cdot \cos\theta \cdot N_{y'}^T$$

$$
\begin{aligned}
M^{T}_{xy} &= \frac{\Delta T}{2}\cdot\sum_{k=1}^{n}(\hat{Q}^{k}_{16}\cdot\alpha^{k}_{x}+\hat{Q}^{k}_{26}\cdot\alpha^{k}_{y}+\hat{Q}^{k}_{66}\cdot\alpha^{k}_{xy})\cdot[(z^{'}_{k}+R\cdot\cos\theta)^{2} \\
&\qquad -(z^{'}_{k-1}+R\cdot\cos\theta)^{2}] \\
&= \frac{\Delta T}{2}\cdot\sum_{k=1}^{n}(\hat{Q}^{k}_{16}\cdot\alpha^{k}_{x}+\hat{Q}^{k}_{26}\cdot\alpha^{k}_{y}+\hat{Q}^{k}_{66}\cdot\alpha^{k}_{xy})\cdot[(z^{'\,2}_{k}-z^{'\,2}_{k-1}) \\
&\qquad +2\cdot R\cos\theta\cdot(z^{'}_{k}-z^{'}_{k-1})] \\
&= M^{T}_{xy'}+R\cdot\cos\theta\cdot N^{T}_{xy'}
\end{aligned}
$$

The equations above can also be written as:

$$
\begin{aligned}
&[N^{T}_{x-y}]=[N^{T}_{x'-y'}] \\
&[M^{T}_{x-y}]=[M^{T}_{x'-y'}]+R\cdot\cos\theta\cdot[N^{T}_{x'-y'}]
\end{aligned}
\tag{3.10}
$$

The above equations confirm that the thermal induced forces remain the same and the thermal induced moments contain a part of moments due to axis translation.

3.4.4 Overall Thermal Induced Force and Moment

To obtain the overall thermal induced force and moment of the composite circular tube, the equations above need to be integrated over the entire length of the circumference of the tube. They are expressed as:

$$
\begin{aligned}
\overline{N}^{T}_{x} &= \int_{0}^{2\pi} N^{T}_{x}\cdot R\cdot d\theta \\
\overline{N}^{T}_{y} &= \int_{0}^{2\pi} N^{T}_{y}\cdot R\cdot d\theta \\
\overline{N}^{T}_{xy} &= \int_{0}^{2\pi} N^{T}_{xy}\cdot R\cdot d\theta
\end{aligned}
\tag{3.11}
$$

and

$$\overline{M}_x^T = \int_0^{2\pi} M_x^T \cdot R \cdot d\theta$$

$$\overline{M}_y^T = \int_0^{2\pi} M_y^T \cdot R \cdot d\theta \tag{3.12}$$

$$\overline{M}_{xy}^T = \int_0^{2\pi} M_{xy}^T \cdot R \cdot d\theta$$

Then, the closed form solution of overall thermal induced force of the composite tubular beam is provided in Appendix A.

3.5 In-Plane Stress Calculation

The ply total strain is obtained using mid-plane strain, $[\varepsilon^0]$ plus mid-plane curvature, $[\kappa]$ multiplying by the ply coordinate. Then, the mechanical strain is acquired by subtracting the thermal strain from the total strain. Finally, the ply stress can be obtained by multiplying the $[\hat{Q}]$ matrix of the ply with the mechanical strain. It can be expressed as below:

$$[\varepsilon_{x-y}^{Total}]_k = [\varepsilon^0] + (R + z') \cdot \cos\theta \cdot [\kappa] \tag{3.13}$$

$$[\varepsilon_{x-y}^{M}]_k = [\varepsilon_{x-y}^{Total}]_k - [\alpha_{x-y}]_k \cdot \Delta T \tag{3.14}$$

$$[\sigma_{x-y}]_k = \left[\widehat{Q}\right]_k \cdot [\varepsilon_{x-y}^{M}]_k \tag{3.15}$$

The computing procedure of the thermal induced stresses of composite tubular structures is shown in the following flow chart, Fig. 3.5.

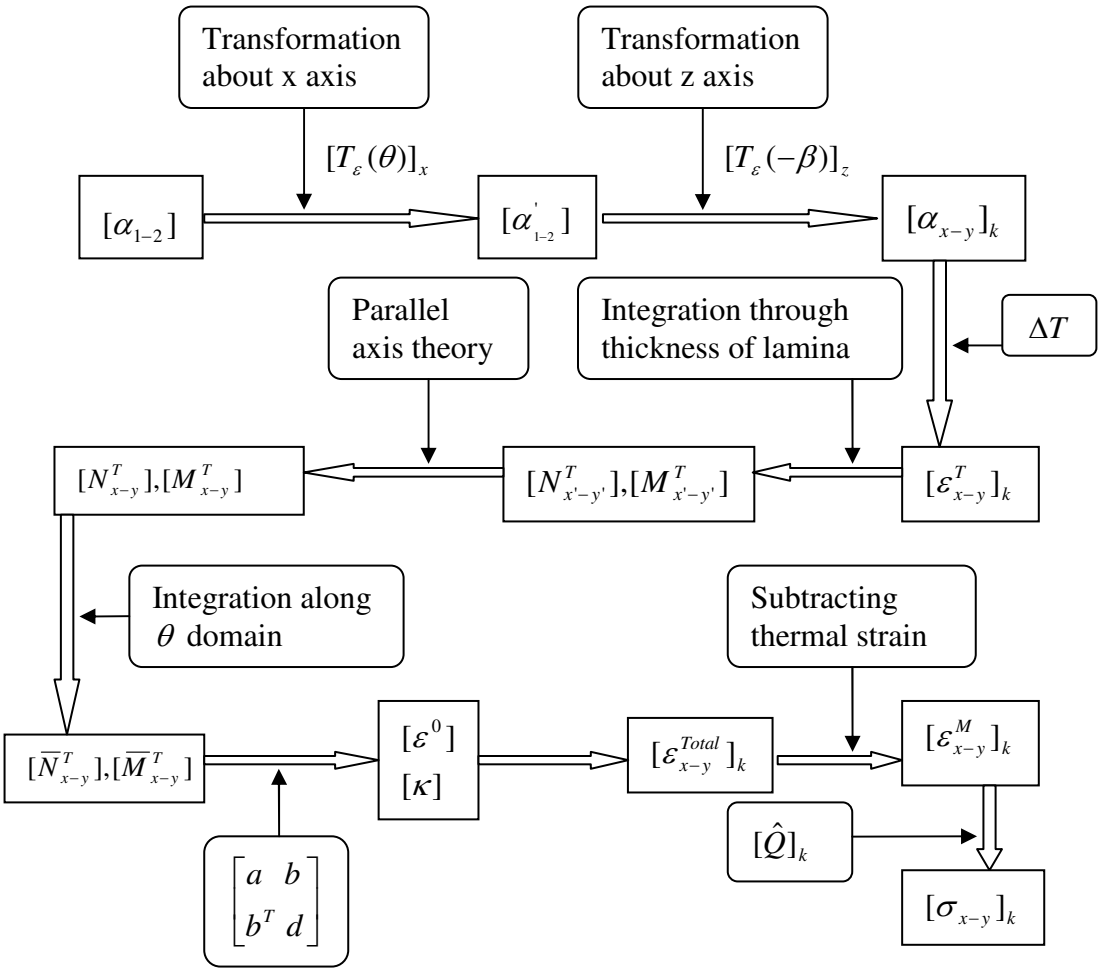

Fig. 3.5 Procedure flow chart of in-plane stress calculation.

CHAPTER 4

FINITE ELEMENT ANALYSIS

In order to confirm the accuracy of the present method, finite element method was used here to make the comparison of the results obtained from the analytical close form solution. In general, the behavior of the structures subjected to various loadings can be well defined using finite element analysis, as long as the element type, meshing, and boundary conditions are set up appropriately. In this chapter, two 3-D finite element models were generated using commercial software, ANSYS 10.0. One is for rectangular beam, the other for tubular beam. The models are created as an input ANSYS code, which is provided in Appendix C.

4.1 Composite Tubular Beam Model

The 3D model shown in Fig. 4.1 is built using SOLID 46, which is a 3D 8-node layered structural solid element shown in Fig. 4.2. The element is designed to model layered thick shells or solids, and allows up to 250 various material layers. The element has three degrees of freedom on each node: translations on nodal x, y, and z directions.

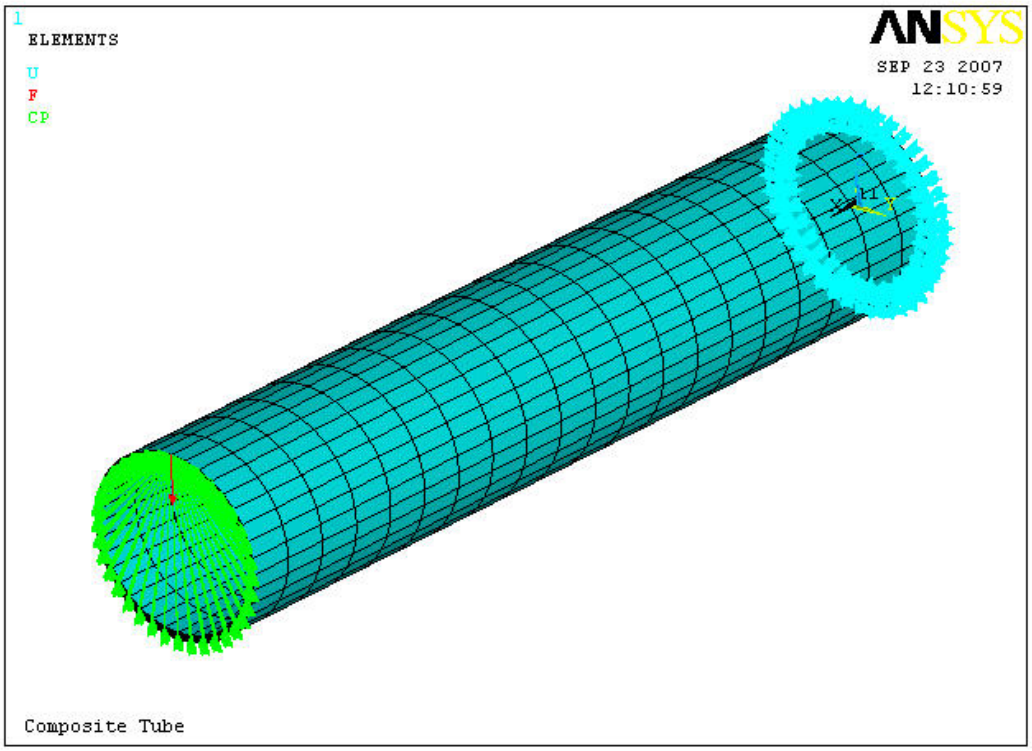

Fig.4.1 The mesh and boundary condition of the finite element tube model

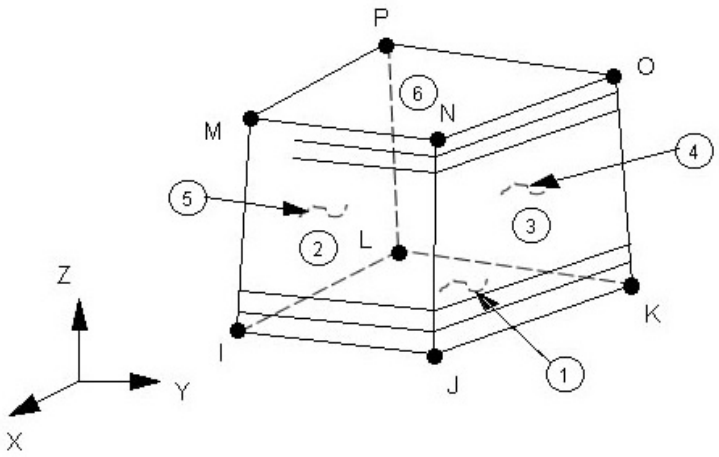

Fig. 4.2 SOLID 46 Element Geometry

4.1.1 Model Description

This 3D model fully contains 11,520 8-node brick elements and 12,852 nodes. Refer to Fig. 4.1, for the laminate thick direction, one element represents a single layer of laminate of the tube. As shown in Fig. 4.1, the circumference was divided to 36 elements, and 20 elements were used in the length direction of the tube on each layer.

4.1.2 Boundary Condition

The boundary condition of the tube was set up as a cantilever beam structure. All the nodes on the cross-section at one end were constrained for all three degrees of freedom to prevent rigid body motion. On the other end, a 10 lb point load downward to the z direction is applied on the node located in the top of the circumference. To ensure plane remaining plane after deformation, all the nodes on this surface is coupled to the node, which the load applied to, in z direction using CP command.

4.2 Composite Rectangular Beam Model

This 3D composite rectangular beam model is similarly generated using SOLID 46 element.

4.2.1 Model Description

As shown in Fig. 4.3, the model is constructed by 6,400 8-node brick elements with total 7,667 nodes. Identical to the tube model, each element represents one layer of

the laminate in the thickness direction. Furthermore, there are 10 by 40, in width and length direction respectively, elements in each layer of the laminate.

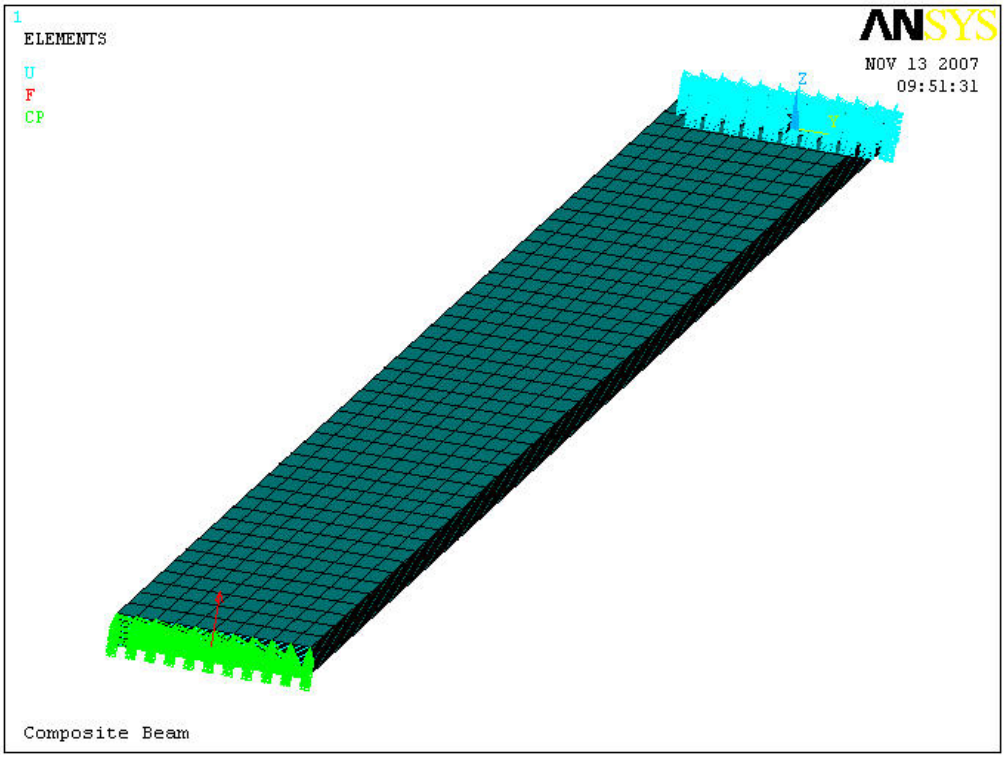

Fig. 4.3 Mesh and Boundary Condition of the Finite Element Beam Model

4.2.2 Boundary Condition

Similar to the circular tube model, all nodes on the cross-sectional surface in the fixed end of the cantilever beam are constrained in three degrees of freedom, UX, UY, and UZ, in order to avoid the rigid body motion. Further, a point load upward to z direction is applied on the node located in the middle of the cross sectional plane in the

free end. All the nodes on the plane with load application are coupled together using CP command to enforce the movement in the z direction.

4.3 Verification of Finite Element Model

In order to correctly make comparison with the analytical results, the validity of the finite element model has to be first checked. The solution of the maximum displacement for cantilever beam made of isotropic material under a transverse load at its free end is known in literature. Hence, it is suitable to compare the maximum displacement of the finite element model using isotropic material. The maximum displacement of a cantilever beam under transverse load is given as:

$$w_{\max} = \frac{PL^3}{3EI} + \frac{3PL}{2GA} \tag{4.1}$$

where

$$I = \frac{\pi}{4}(R_o^{\,4} - R_i^{\,4}) \quad , \quad A = \pi (R_o^{\,4} - R_i^{\,4}) \qquad \text{for Tubular Beam}$$

$$I = \frac{bh^3}{12} \quad , \quad A = bh \qquad \text{for Rectangular Ream}$$

In the above equations, E is the elastic modulus of the material, I is the moment of inertia, P is the applied load, L is the length of the beam, G is the shear modulus of

the material, and A is the area of the cross section. Data and material properties of the isotropic material are given in Table 4.1.

Table 4.1 Data and Properties of the Model Using Isotropic Material

Properties	Circular Tube	Rectangular Beam
Elastic Modulus, E (Msi)	30	
Shear Modulus, G (Msi)	11.6	
Poisson's Ratio, v	0.3	
Applied Load, P (lb)	10	
Length, L (in)	10	
Radius, R^* (in)	from 1.0 to 0.25	
Width, b (in)		from 1.5 to 0.5
Thickness, t (in)	0.08	
Element Type	SOLID 46	

* $R = \frac{R_o + R_i}{2}$

A comparison of the results between FEM and the present method is listed in Table 4.2 and Table 4.3. The difference between analytical results and finite element method results is no more than 2%. This clearly proves the validity of the finite element model using isotropic material, and gives confidence enough to apply these two models in composite materials.

Table 4.2 Comparison of Free-end Displacement between Analytical Solution and FEM results for the Tube

radius, R (in)	Displacement in free end (in)		% Difference
	Analytical solution	FEM result	
1	-4.67E-04	-4.73E-04	1.29%
0.75	-1.08E-03	-1.08E-03	0.49%
0.5	-3.57E-03	-3.56E-03	-0.03%
0.25	-2.77E-02	-2.76E-02	-0.30%

Table 4.3 Comparison of Free-end Displacement between Analytical Solution and FEM results for the Rectangular Beam

width, b (in)	Displacement in free end (in)		% Difference
	Analytical solution	FEM result	
1.5	-1.74E+00	-1.70E+00	1.91%
1.25	-2.08E+00	-2.05E+00	1.65%
1	-2.60E+00	-2.57E+00	1.39%
0.75	-3.47E+00	-3.43E+00	1.14%
0.5	-5.21E+00	-5.16E+00	0.88%

CHAPTER 5

RESULTS COMPARISON AND PARAMETRIC STUDIES

In this chapter, in order to confirm the accuracy of present methods, the comparison between the results obtained from analytical solution and finite element solution is made. In addition, the geometries of the beam and the tube, fiber orientation, and stacking sequence play an important role in the stiffness of the composite structures. The effects of these on the distribution of in-plane stresses and interlaminar stress are also discussed. In this study, Carbon/Epoxy AS4/3501-6 is chosen as the material of both rectangular beam and circular tube. Its material properties are shown in Table 5.1.

Table 5.1. Material properties of composite laminate
Carbon/Epoxy AS4/3501-6 [15]

Carbon/Epoxy AS4/3501-6	
E_1	21.3 E6 psi
$E_2 = E_3$	1.5 E6 psi
$\nu_{12} = \nu_{13} = \nu_{23}$	0.27
$G_{12} = G_{13} = G_{23}$	1.0 E6 psi
α_1	-0.5 E-6 $in/in/^{\circ}F$
$\alpha_2 = \alpha_3$	15E-6 $in/in/^{\circ}F$
t_{ply}	0.005 in

5.1 In-Plane Stresses of Rectangular Laminated Composite Beam

The in-plane stresses of the rectangular composite beam with temperature effect can be obtained by using the approach presented in Chapter 2. This beam is cantilevered in one end, and a transverse force, q = 1 lb/in, is applied upward in the other end. Additionally, the stacking sequence of the laminate is $[\pm 45/90/0/90/0/\pm 45]_S$, and the temperature is assumed 50 $°F$ higher than the stress-free temperature(assumed to be at the room temperature). The comparison of the results between analytical solution and finite element analysis is shown in Fig. 5.1. The deformation and the contour plot of the axial stress distribution of the composite beam are shown in Fig. 5.2.

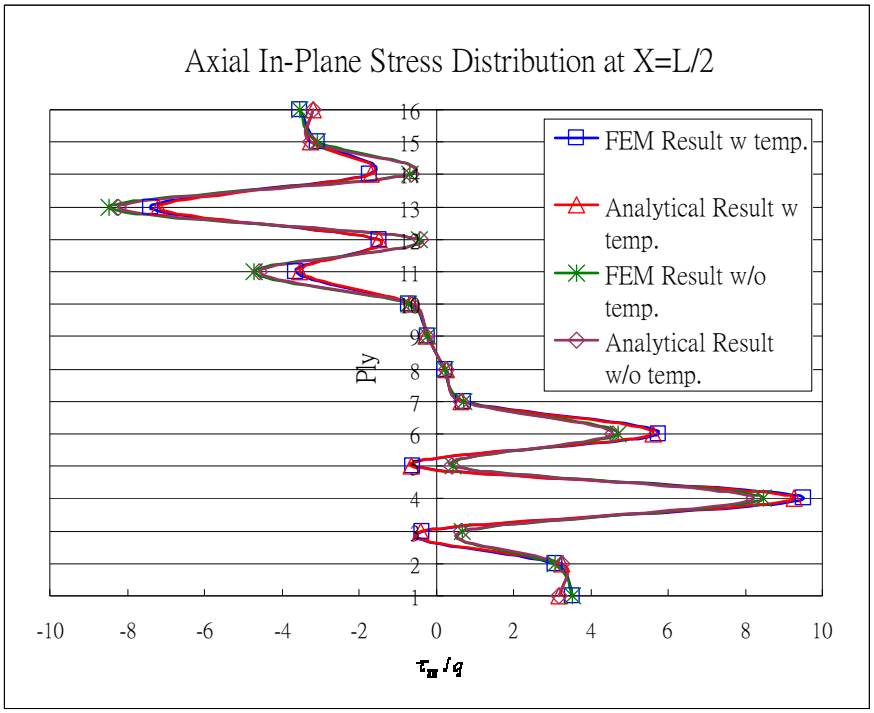

Fig. 5.1 Normalized σ_x distribution across the thickness of the beam.

As shown in Fig. 5.1, the in-plane stress of each layer obtained by finite element method and the present analytical method agree very well. Fig. 5.1 also indicates that the in-plane stress is symmetric with respect to the mid-plane of the laminate. However, with temperature included, the stress distribution across the thickness is no longer symmetric with respect to the mid-plane of the laminate. Moreover, it is also found that the outer $0°$-ply exhibits higher temperature induced stress compared to the inner $0°$-ply.

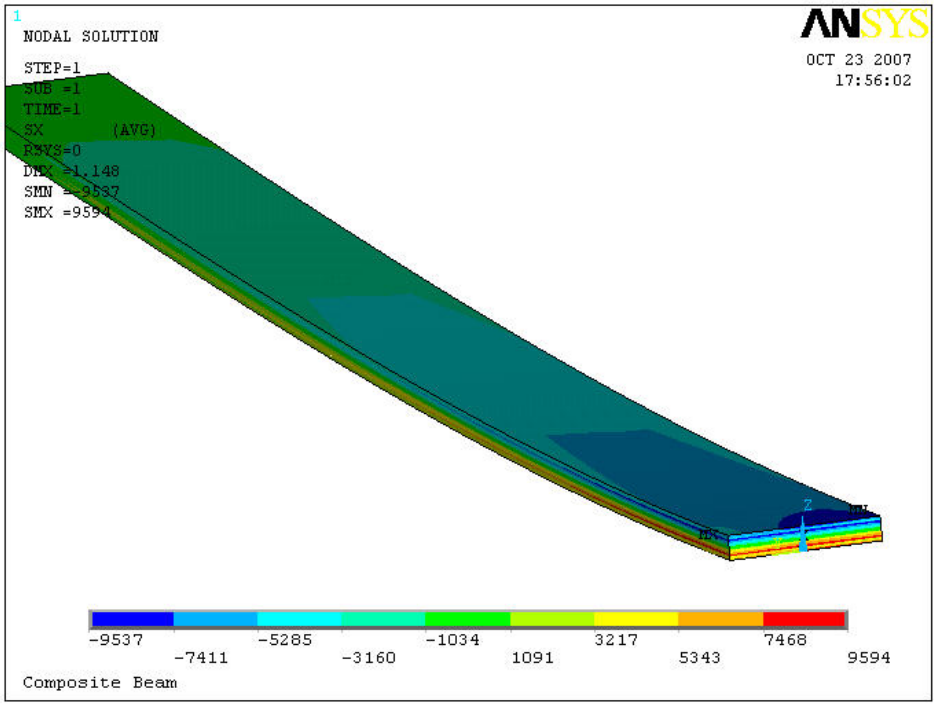

Fig. 5.2 Contour plot of axial in-plane stress distribution

5.2 Interlaminar Shear Stress of Rectangular Laminated Composite Beam

In Chapter 2, it is concluded that thermal induced force and moment do not affect the distribution of interlaminar shear stresses of the rectangular composite beam, which is cantilevered in one end, and under a transverse load in the other end. The transverse load, q here is assumed to be 1 lb/in, and the laminate is with $[\pm 45/90/0/90/0/\pm 45]_S$ lay-up. Further, 50 $°F$ of temperature change is assumed. Fig. 5.3 shows a comparison of the results between FEM model and analytical model.

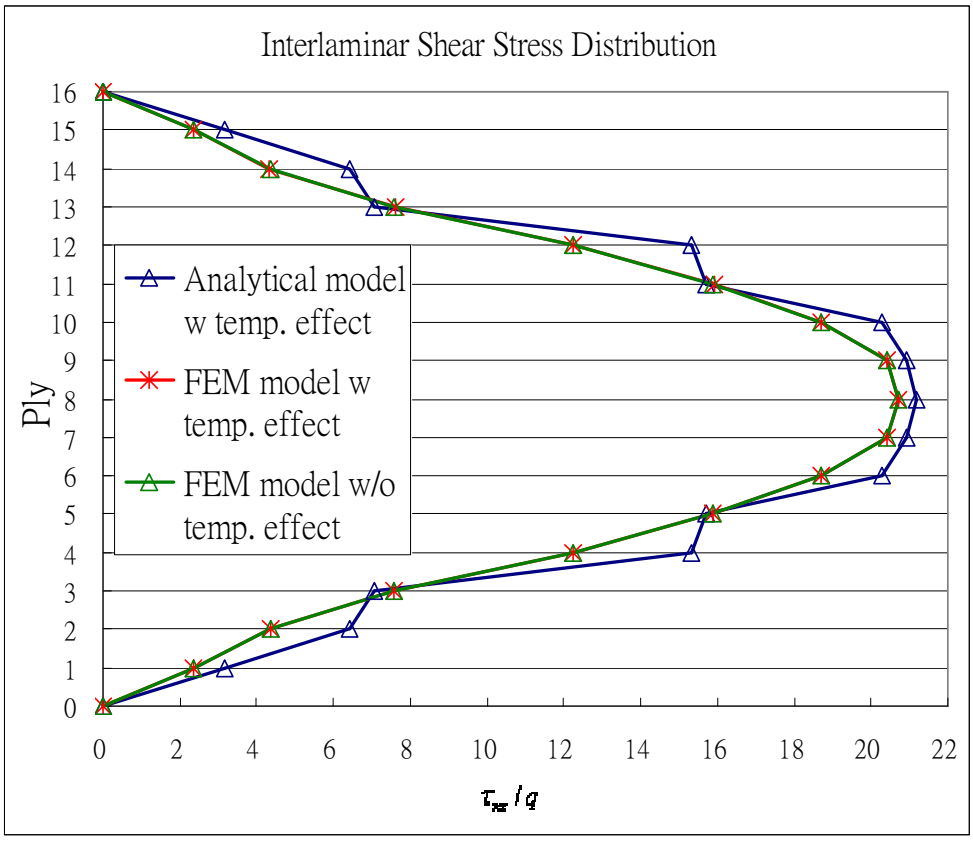

Fig. 5.3 Normalized τ_{xz} distribution across the thickness of the beam.

5.3 Axial In-Plane Stresses of Tubular Laminated Composite Beam

The in-plane stress of the laminated composite tube along the axial direction (x-direction) under temperature environment is discussed in Chapter 3. In this case, the stacking sequence of the composite tube is $[\pm 45/90/0/90/0/\pm 45]_S$ .Further, the tube is cantilevered on one side, and subjected a transverse load, q = 10 lb on the free end. The comparisons about σ_x of different layers of the laminate obtained from the finite element model and analytical solution are shown in following figures. Fig. 5.4 through 5.7 shows the in-plane stresses of $45°$, $-45°$, $90°$, and $0°$ ply around the circumference of the tube, respectively. Fig. 5.8 through 5.11 depicts the stress contour of σ_x for each ply. As shown, the higher stress is located at the upper surface of $0°$ ply for any given x position. It is also noted that all of the stresses without temperature are zero at $\theta = 90°$ and $270°$ where the neutral axis is located.

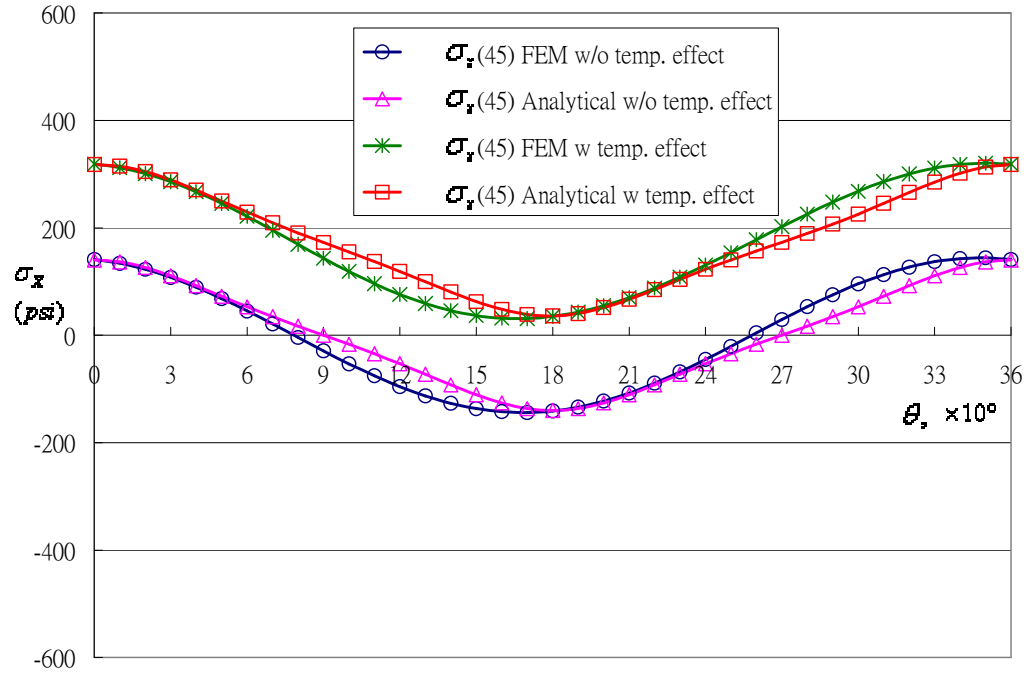

Fig. 5.4 σ_x in $45°$ ply of the laminate around the circumference of the tube

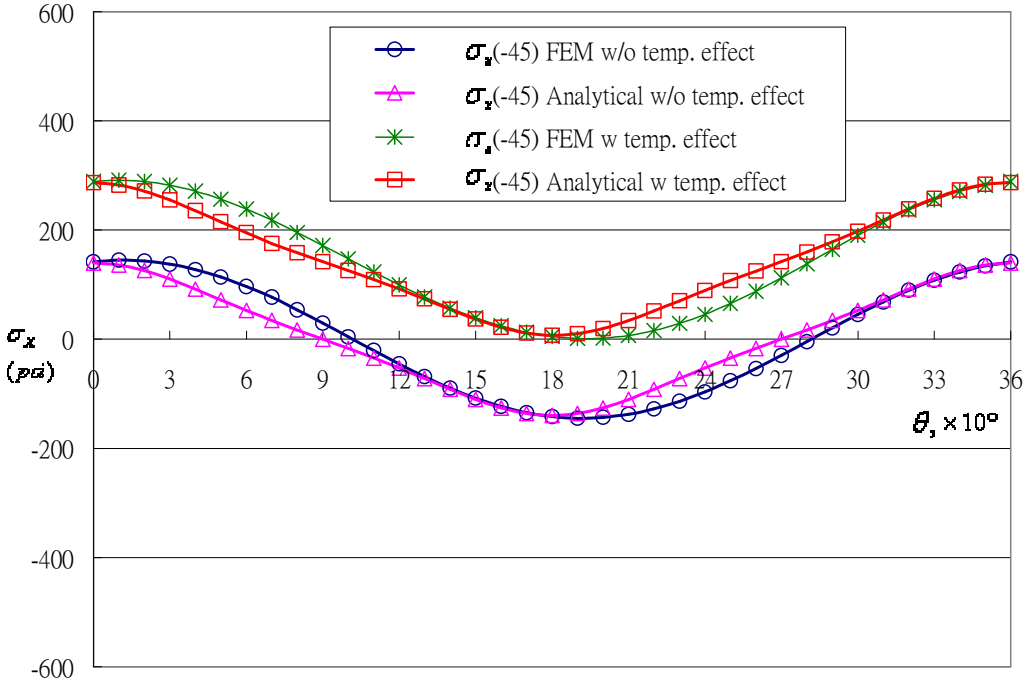

Fig. 5.5 σ_x in $-45°$ ply of the laminate around the circumference of the tube

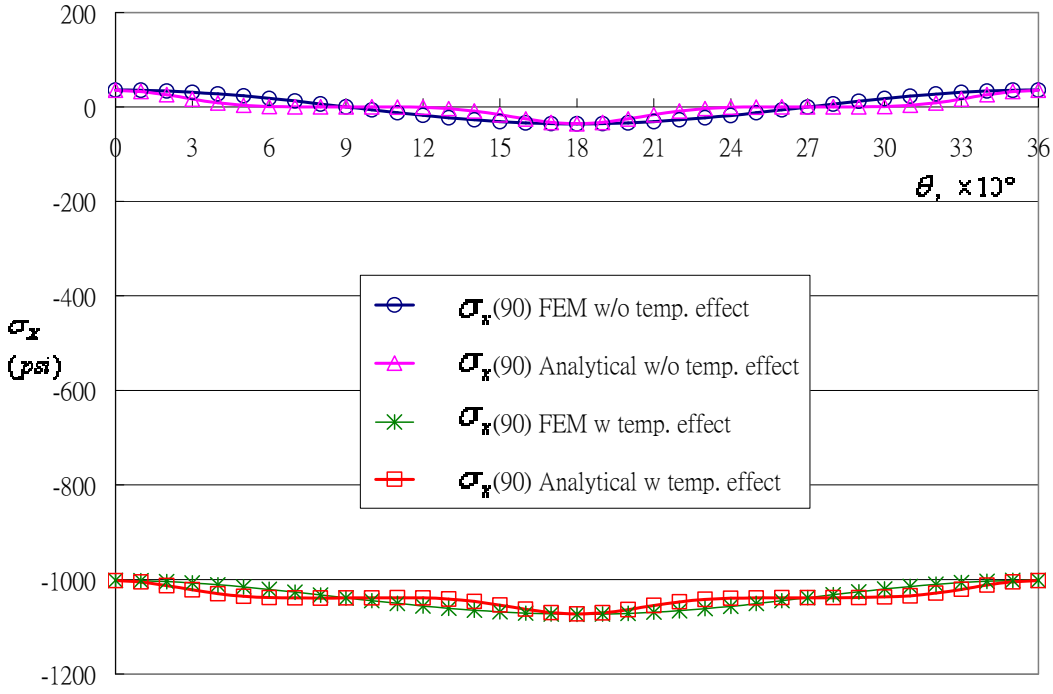

Fig. 5.6 σ_x in $90°$ ply of the laminate around the circumference of the tube

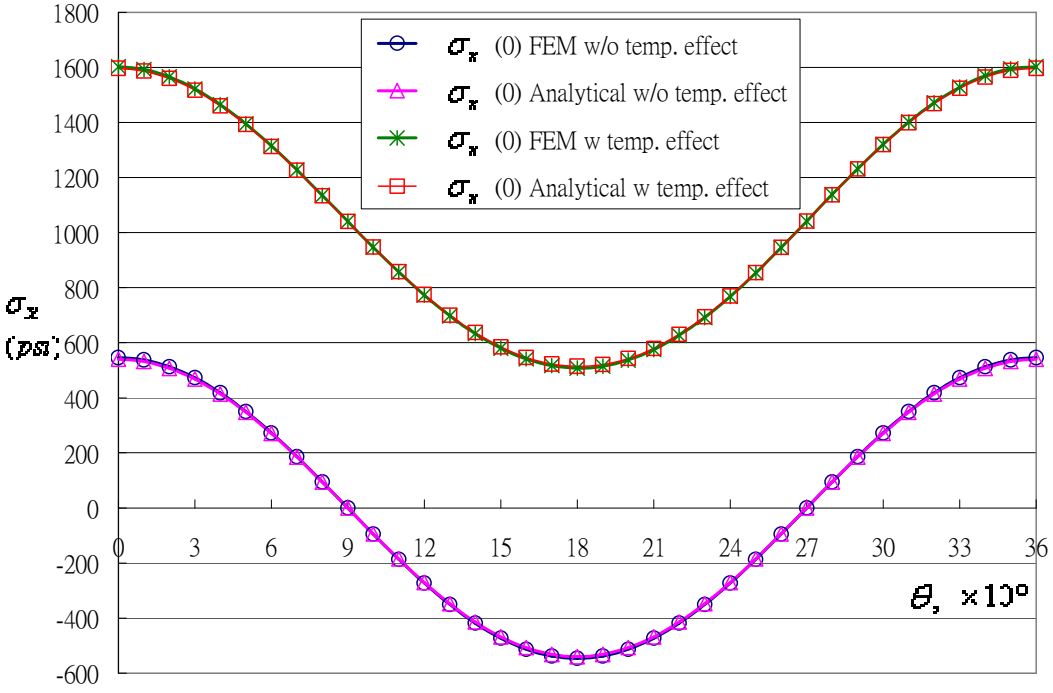

Fig. 5.7 σ_x in $0°$ ply of the laminate around the circumference of the tube

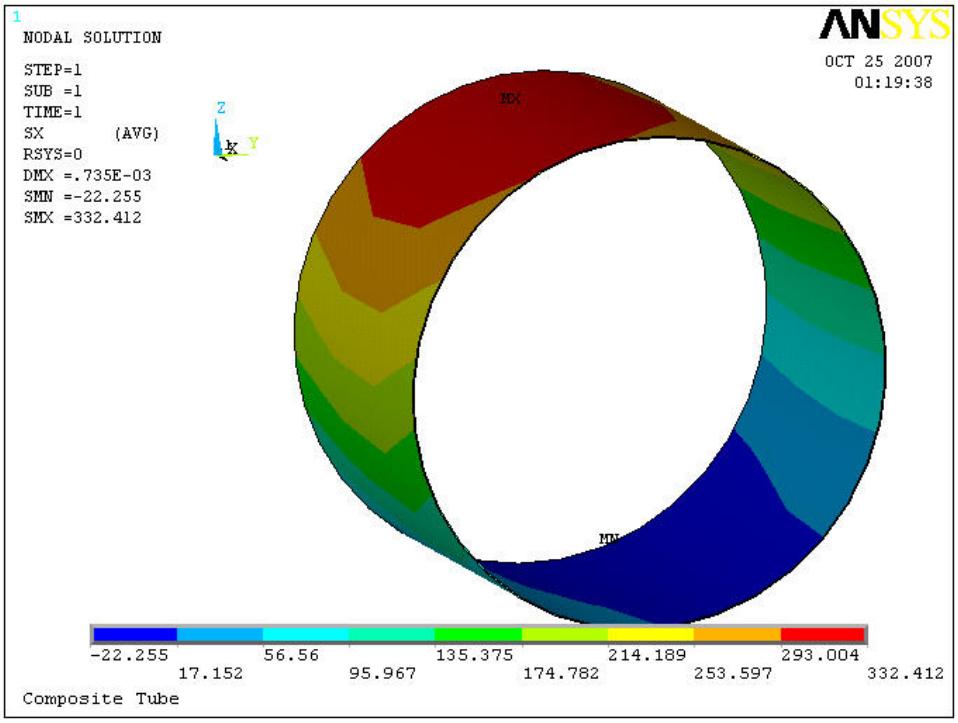

Fig. 5.8. Contour plot of the σ_x distribution for $45°$ ply with $50°F$

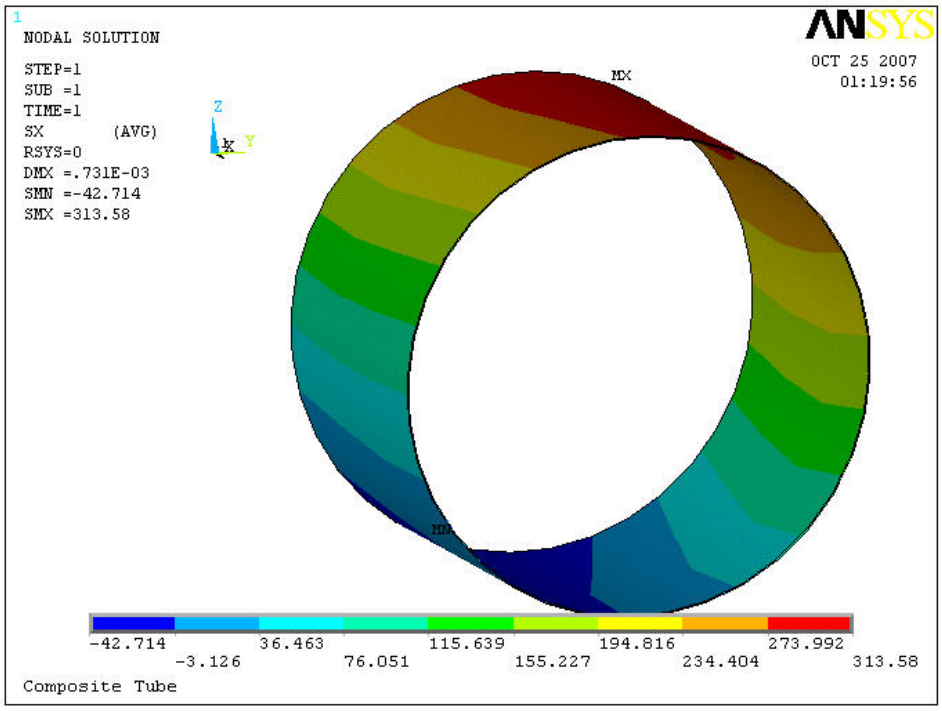

Fig. 5.9 Contour plot of the σ_x distribution for $-45°$ ply with $50°F$

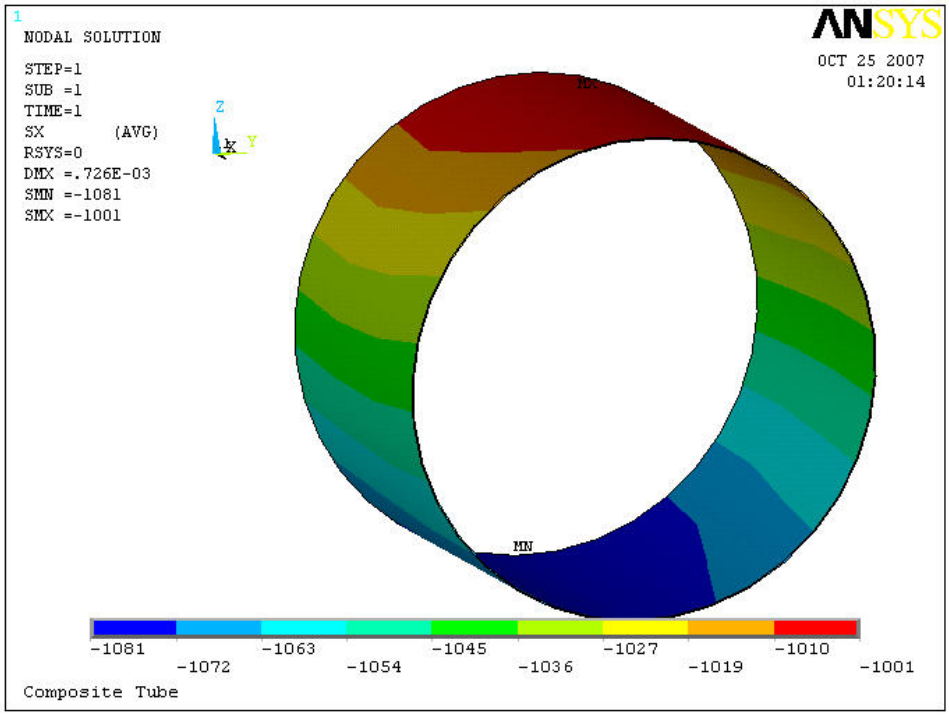

Fig. 5.10 Contour plot of the σ_x distribution for $90°$ ply with $50°F$

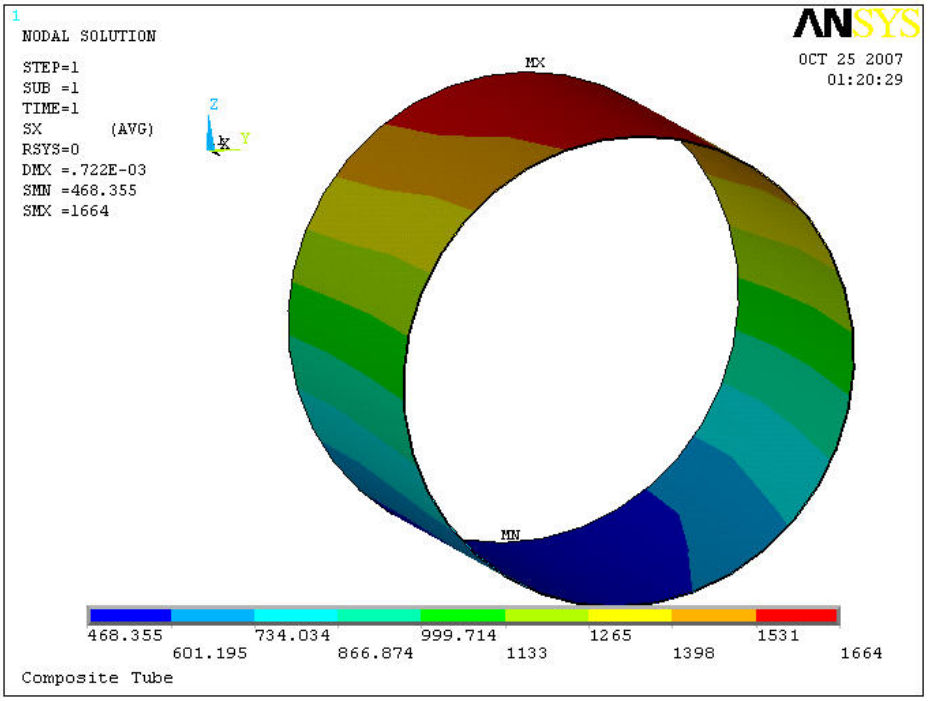

Fig. 5.11 Contour plot of the σ_x distribution for $0°$ ply with $50°F$

5.4 Stacking Sequence Effect

In this section, the effect of stacking sequence of the laminate on the axial in-plane stress is studied for both rectangular beam and circular tube by using the present analytical model. To examine the effects, three laminates with the same fiber orientations, but different stacking sequences are considered. $[\pm 45/90/0/90/0/\pm 45]_S$, $[\pm 45/90_2/\pm 45/0_2]_S$, and $[\pm 45/90_2/\pm 45/0_2]_{2T}$ are the three different lay ups chosen for study. The various results of the in-plane stresses for these three cases are observed.

5.4.1 Rectangular Beam

Fig. 5.12 through 5.14 shows axial in-plane stresses across the thickness of the beams with the three different lay-ups described above. The results indicate that the higher stress occurs in laminate with more $0°$ ply placed away from the mid-plane of the laminate.

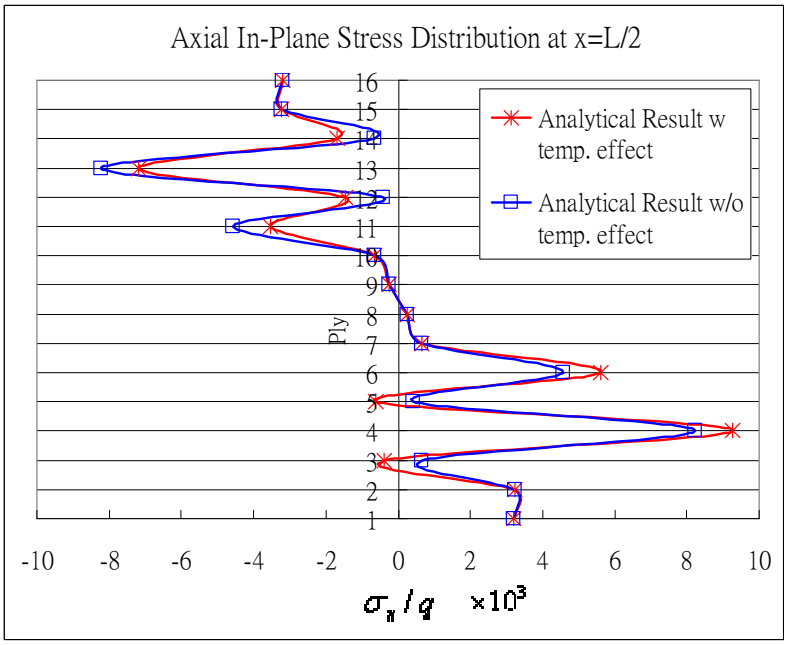

Fig. 5.12 Normalized σ_x distribution for $[\pm 45/90/0/90/0/\pm 45]_S$ lay-up

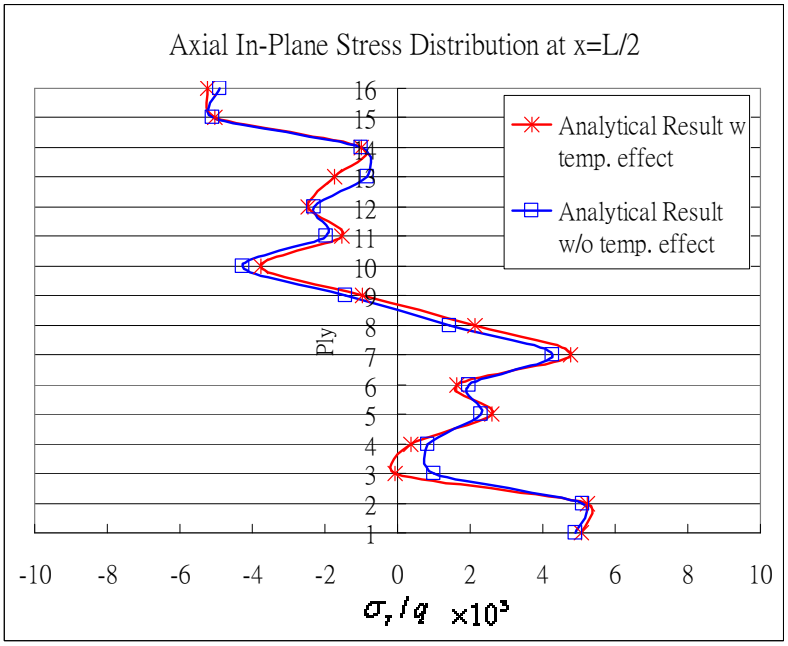

Fig. 5.13 Normalized σ_x distribution for $[\pm 45/90_2/\pm 45/0_2]_S$ lay-up

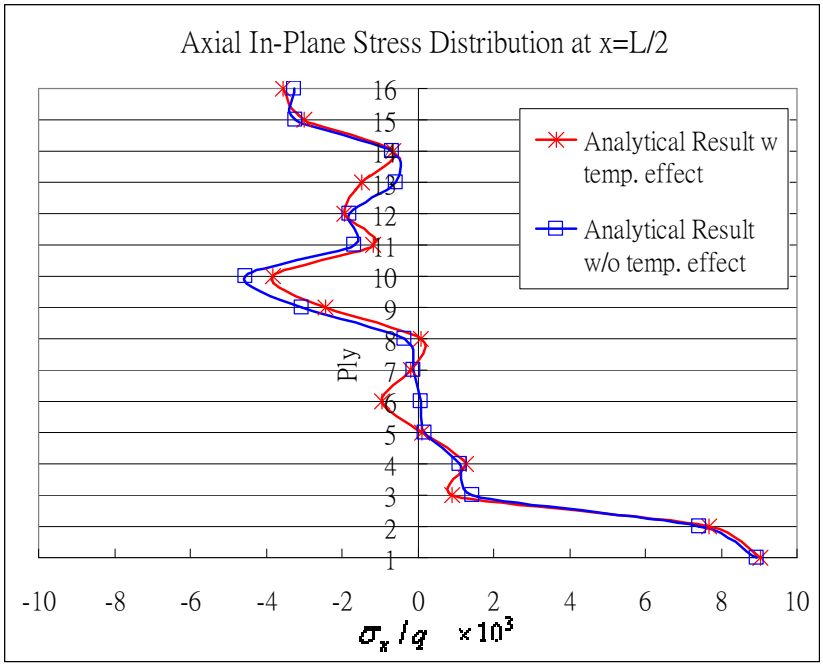

Fig. 5.14 Normalized σ_x distribution for $[\pm 45/90_2/\pm 45/0_2]_{2T}$ lay-up

5.4.2 Tubular Beam

Since the composite tubular cantilever beam studied here is subjected a downward transverse load on the free end, the maximum tensile stress is known occurring on the upper half part of the tube with $\theta = 0$ in θ domain. Hence, the variation of the axial in-plane stress across the thickness of the laminate in $\theta = 0$ due to thermal effect is taken to be observed. The increased axial in-plane stress due to thermal expansion for three laminates with various stacking sequences is shown in Fig. 5.15, 5.16, and 5.17, respectively.

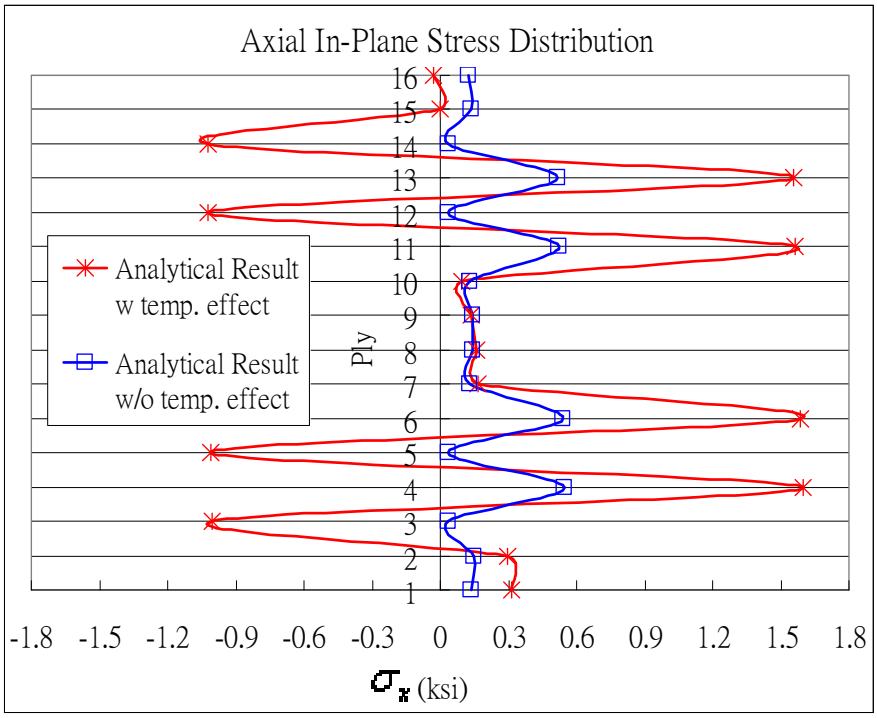

Fig. 5.15 σ_x distribution for tube with $[\pm 45/90/0/90/0/\pm 45]_S$ lay-up

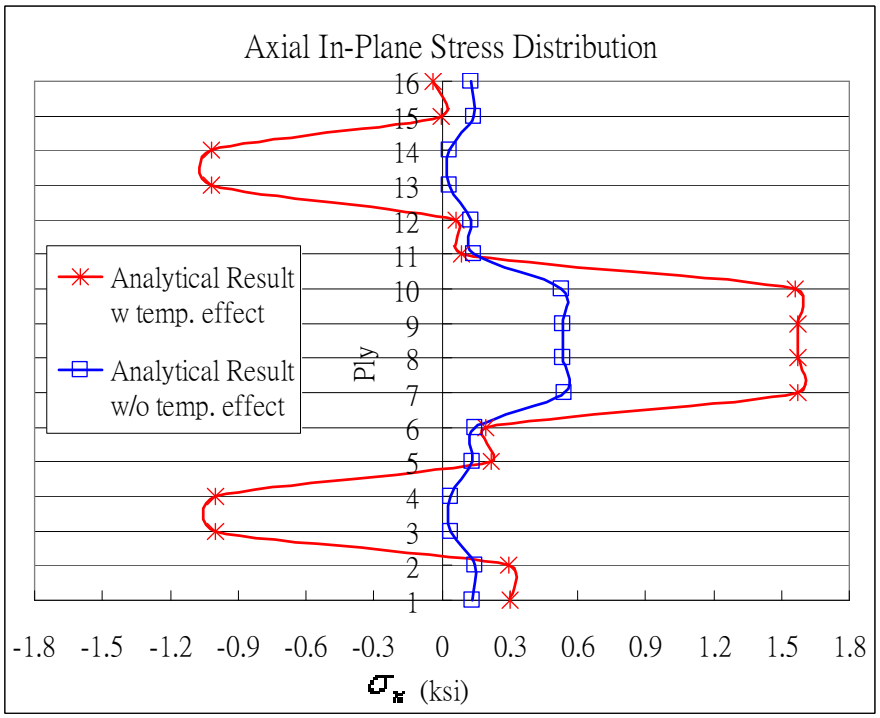

Fig. 5.16 σ_x distribution for tube with $[\pm 45/90_2/\pm 45/0_2]_S$ lay-up.

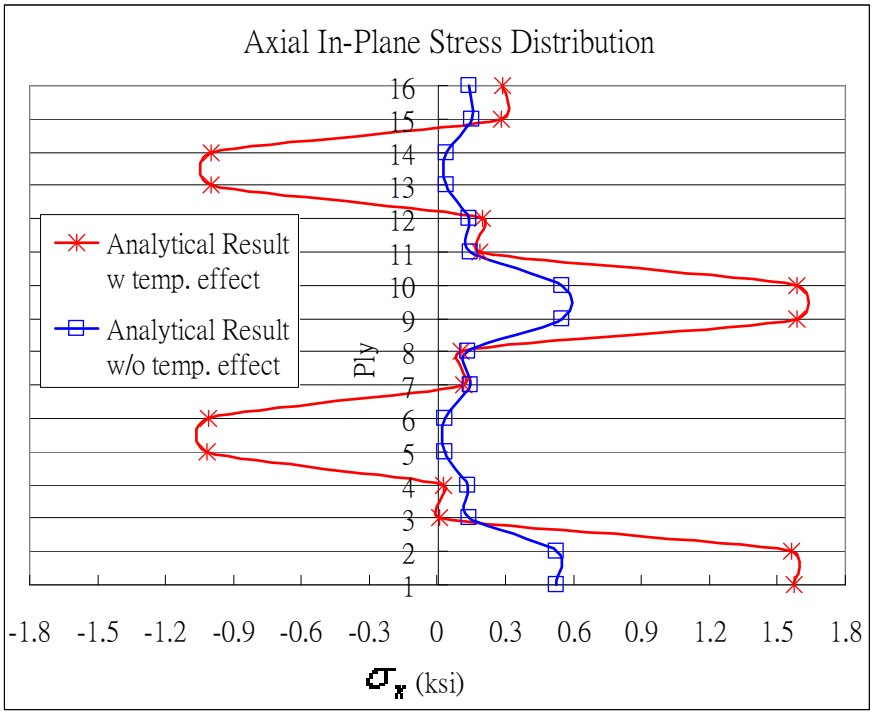

Fig. 5.17 σ_x distribution for tube with $[\pm 45/90_2/\pm 45/0_2]_{2T}$ lay-up

From the above results, it is observed that varying stacking sequence does affect the magnitude of axial in-plane stress in each ply for the rectangular beam. For the tubular bean, σ_x stress variation across the wall thickness is small since the bending is with respect to the mid-axis of the tube. It is also shown in the figures that the significant σ_x is induced in $0°$ and $90°$ plies when under temperature environment. Little thermal stresses are induced in $\pm 45°$ plies. In addition, the increased in-plane stresses due to thermal expansion are little affected by stacking sequence since the inducing of in-plane thermal stresses are due to the mismatch of the axial thermal expansion between each ply of the laminate.

5.5 Fiber Orientation Effect

The directional dependence of laminated composite material is one of the important properties in the design of composite structure. In this section, the effect of fiber orientation of laminate on the axial in-plane stress is studied. Four symmetric lay-ups with $\pm\theta°$ and $0°$ are considered. $60°$, $70°$, $80°$, and $90°$ are chosen as the value of fiber orientations of the laminate. The following figures represent the axial in-plane stresses of the tubes with these four different fiber orientations.

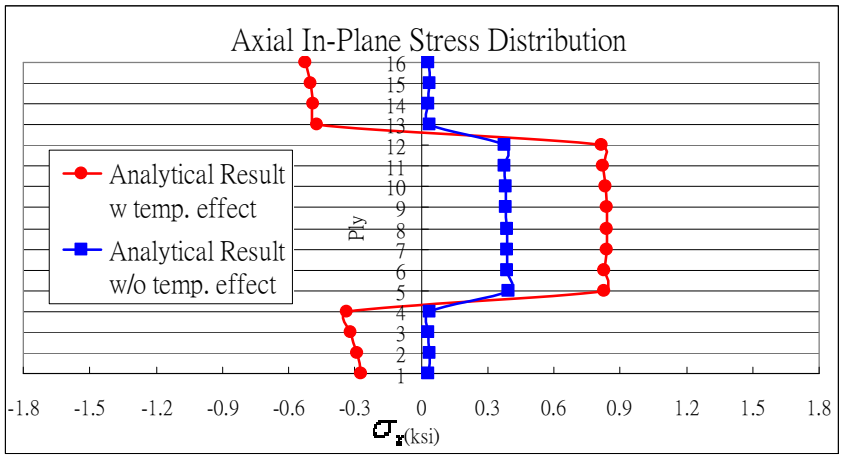

Fig. 5.18 σ_x distribution for tube with $[\pm 60_2 / 0_4]_S$ lay-up.

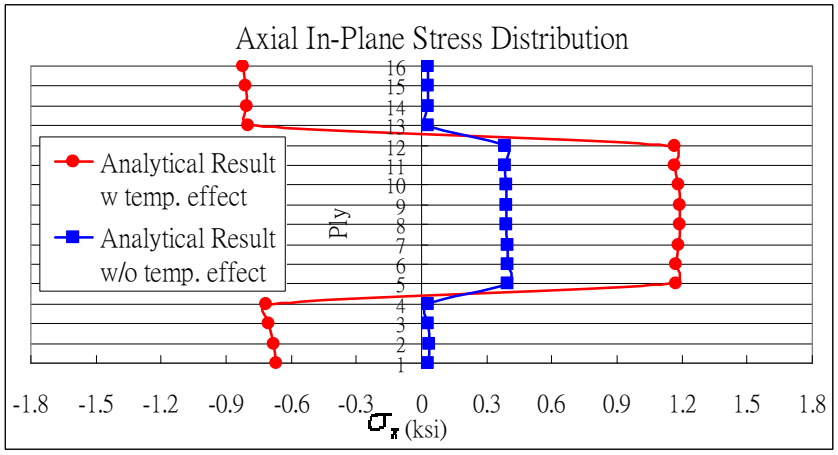

Fig. 5.19 σ_x distribution for tube with $[\pm 70_2 / 0_4]_S$ lay-up.

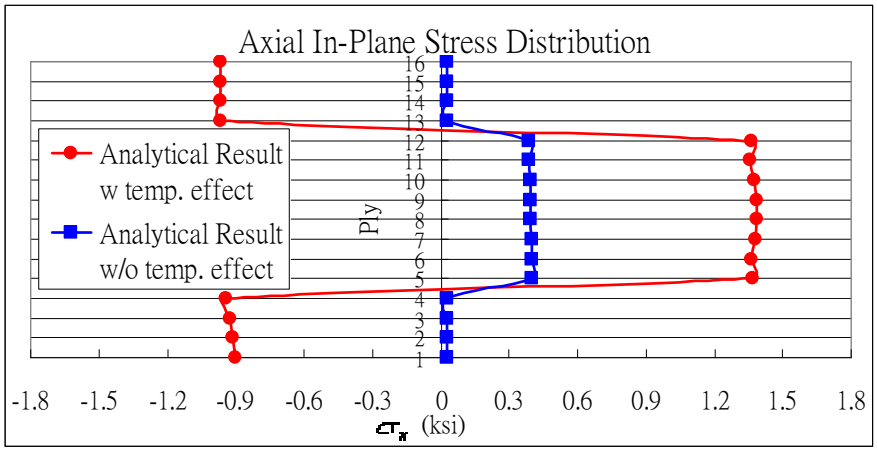

Fig. 5.20 σ_x distribution for tube with $[\pm 80_2 / 0_4]_S$ lay-up.

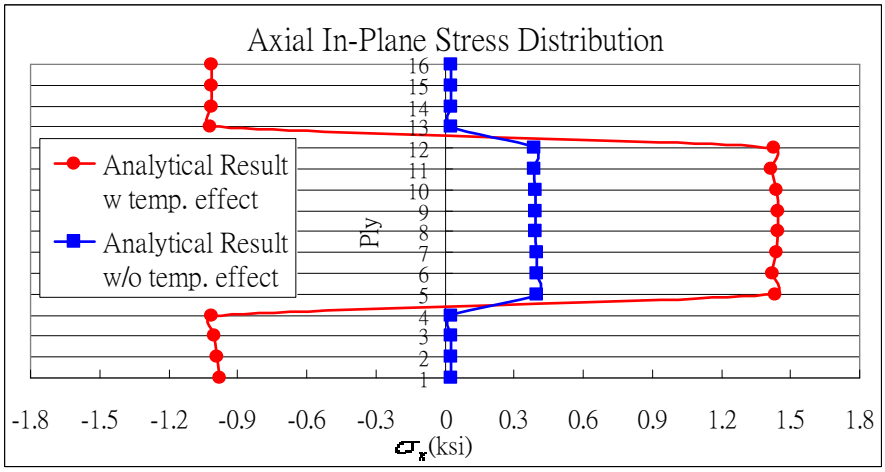

Fig. 5.21 σ_x distribution for tube with $[\pm 90_2 / 0_4]_S$ lay-up.

Table 5.2 Comparison of increased stresses in $0°$ ply due to thermal effect

Stacking sequence	Max. tensile stress with thermal effect	Max. tensile stress w/o thermal effect	Increased in-plane stress due to thermal effect
$[\pm 60_2 / 0_4]_S$	841.39 psi	393 psi	448.39 psi
$[\pm 70_2 / 0_4]_S$	1190.6 psi	399.1 psi	791.5 psi
$[\pm 80_2 / 0_4]_S$	1385.9 psi	401.18 psi	984.72 psi
$[\pm 90_2 / 0_4]_S$	1448.1 psi	401.69 psi	1046.41 psi

The results indicate that the fiber orientation of the laminate plays an important role in the thermal induced in-plane stresses. From the results, it is seen that the constituent of $0°$ and $90°$ plies exhibits the greatest significant thermal effect.

CHAPTER 6

CONCLUSIONS

Analytical closed-form expressions to analyze thermal induced stresses for laminated composite beams with rectangular and tubular cross-sections were developed. All derivations were based on modification of conventional lamination theory by using parallel axis theorem. For the circular composite tube, the stiffness matrices and thermal induced loads and moments were derived. The variation of stiffness along the contour is included. For rectangular beam, the narrow width of the beam is considered. All results of thermal stresses obtained from analytical model were compared with results obtained from finite element model built with the commercial software package, ANSYS 10. From this study, the following conclusions can be made.

For cantilevered composite beams with rectangular cross-section, we have

- The axial in-plane stresses of each ply obtained by the current developed method exhibit an excellent agreement with the results obtained from finite element analysis.
- The interlaminar shear stresses of each ply calculated from present method are in a good agreement with the results obtained from finite element analysis.

- The interlaminar shear stress due to the transverse load does not appear to have any influence by the presence of uniform temperature.
- While the set of plies is given, the stacking sequence of the laminate does not significantly affect the increased axial in-plane stress of the rectangular beam due to the thermal effect.

For cantilevered composite beams with tubular cross-section, we obtain

- The thermal induced stresses obtained by the present method give an excellent agreement with the finite element results.
- The fiber orientation of the plies plays an important role on the thermal induced in-plane stresses. This is mainly caused by the thermal induced moments. The induced moments are due to the mismatch of the axial thermal expansion between each ply of the laminate.

It is well understood that the analysis of moisture effect for laminated beam is analog to the thermal effect. Hence, the present method is also applicable for the analysis of moisture effect of laminated composite structure.

APPENDIX A

TRANSFORMATIONS OF STIFFNESS MATRIX AND CTE

A.1 Transformation Matrices

In this section, transformation matrices for stress and strain rotated about x-axis and z-axis are listed, respectively.

A.1.1 Stress Transformation Matrices

3D stress transformation matrix rotated a positive angle θ about x-axis is given as:

$$[T_\sigma(\theta)]_x = \begin{bmatrix} 1 & 0 & 0 & 0 & 0 & 0 \\ 0 & c_x^2 & s_x^2 & 2c_x s_x & 0 & 0 \\ 0 & s_x^2 & c_x^2 & -2c_x s_x & 0 & 0 \\ 0 & -c_x s_x & c_x s_x & c_x^2 - s_x^2 & 0 & 0 \\ 0 & 0 & 0 & 0 & c_x & -s_x \\ 0 & 0 & 0 & 0 & s_x & c_x \end{bmatrix} \tag{A.1}$$

where $c_x = \cos\theta$ and $s_x = \sin\theta$.

For plane stress condition, the 2D stress transformation matrix can be reduced into:

$$[T_\sigma(\theta)]_x = \begin{bmatrix} 1 & 0 & 0 \\ 0 & c_x^2 & 0 \\ 0 & 0 & c_x \end{bmatrix} \tag{A.2}$$

Additionally, 3D stress transformation matrix rotated a positive angle β about z-axis is given as:

$$[T_\sigma(\beta)]_z = \begin{bmatrix} c_z^2 & s_z^2 & 0 & 0 & 0 & 2c_z s_z \\ s_z^2 & c_z^2 & 0 & 0 & 0 & -2c_z s_z \\ 0 & 0 & 1 & 0 & 0 & 0 \\ 0 & 0 & 0 & c_z & -s_z & 0 \\ 0 & 0 & 0 & s_z & c_z & 0 \\ -c_z s_z & c_z s_z & 0 & 0 & 0 & c_x^2 - s_z^2 \end{bmatrix} \tag{A.3}$$

where $c_z = \cos\beta$ and $s_z = \sin\beta$

2D stress transformation matrix can be written as:

$$[T_\sigma(\beta)]_z = \begin{bmatrix} c_z^2 & s_z^2 & 2c_z s_z \\ s_z^2 & c_z^2 & -2c_z s_z \\ -c_z s_z & c_z s_z & c_z^2 - s_z^2 \end{bmatrix} \tag{A.4}$$

A.1.2 Stain Transformation Matrices

3D strain transformation matrix rotated a positive angle θ about x-axis is given as:

$$[T_\varepsilon(\theta)]_x = \begin{bmatrix} 1 & 0 & 0 & 0 & 0 & 0 \\ 0 & c_x^2 & s_x^2 & c_x s_x & 0 & 0 \\ 0 & s_x^2 & c_x^2 & -c_x s_x & 0 & 0 \\ 0 & -2c_x s_x & 2c_x s_x & c_x^2 - s_x^2 & 0 & 0 \\ 0 & 0 & 0 & 0 & c_x & -s_x \\ 0 & 0 & 0 & 0 & s_x & c_x \end{bmatrix} \tag{A.5}$$

where $c_x = \cos\theta$ and $s_x = \sin\theta$.

For plane stress condition, the 2D stress transformation matrix can be reduced into:

$$[T_{\varepsilon}(\theta)]_x = \begin{bmatrix} 1 & 0 & 0 \\ 0 & \mathrm{c_x}^2 & 0 \\ 0 & 0 & \mathrm{c_x} \end{bmatrix} \tag{A.6}$$

Additionally, 3D strain transformation matrix rotated a positive angle β about z-axis is given as:

$$[T_{\varepsilon}(\beta)]_z = \begin{bmatrix} \mathrm{c_z}^2 & s_z^2 & 0 & 0 & 0 & \mathrm{c_z}s_z \\ s_z^2 & \mathrm{c_z}^2 & 0 & 0 & 0 & -\mathrm{c_z}s_z \\ 0 & 0 & 1 & 0 & 0 & 0 \\ 0 & 0 & 0 & \mathrm{c_z} & -s_z & 0 \\ 0 & 0 & 0 & s_z & \mathrm{c_z} & 0 \\ -2\mathrm{c_z}\mathrm{s_z} & 2\mathrm{c_z}\mathrm{s_z} & 0 & 0 & 0 & \mathrm{c_x}^2 - s_z^2 \end{bmatrix} \tag{A.7}$$

where $c_z = \cos\beta$ and $s_z = \sin\beta$

2D stress transformation matrix can be written as:

$$[T_{\varepsilon}(\beta)]_z = \begin{bmatrix} c_z^2 & \mathrm{s_z}^2 & \mathrm{c_z}s_z \\ \mathrm{s_z}^2 & c_z^2 & -\mathrm{c_z}s_z \\ -2\mathrm{c_z}s_z & 2\mathrm{c_z}s_z & \mathrm{c_z}^2 - s_z^2 \end{bmatrix} \tag{A.8}$$

A.2 Stress and Strain Transformation from Material (1-2) Coordinate System to Laminate (x-y) Coordinate System

The transformation of stress and strain from the laminate (x-y) coordinate system to the material (1-2) coordinate system can be expressed as:

$$[\sigma]_{1-2} = [T_\sigma] \cdot [\sigma]_{x-y}$$
$$[\varepsilon]_{1-2} = [T_\varepsilon] \cdot [\varepsilon]_{x-y} \tag{A.9}$$

Rewriting equation A.9, we have:

$$[\sigma]_{x-y} = [T_\sigma]^{-1} \cdot [\sigma]_{1-2}$$
$$[\varepsilon]_{x-y} = [T_\varepsilon]^{-1} \cdot [\varepsilon]_{1-2} \tag{A.10}$$

A.2 Transformation of Stiffness Matrices from Material (1-2) Coordinate System to Laminate (x-y) Coordinate System

The relationship between stress and strain can be written as:

$$[\sigma]_{1-2} = [Q] \cdot [\varepsilon]_{1-2}$$
$$[\sigma]_{x-y} = [\overline{Q}] \cdot [\varepsilon]_{x-y} \tag{A.11}$$

Where, $[Q]$ and $[\overline{Q}]$ are the reduced stiffness matrices of lamina which represent the stress/strain relationship with respect to material (1-2) coordinate system and laminate (x-y) coordinate system, respectively.

From equation A.9, A.10, and A.11, we have:

$$[\sigma]_{x-y} = [T_\sigma]^{-1} \cdot [Q] \cdot [\varepsilon]_{1-2} = [T_\sigma]^{-1} \cdot [Q] \cdot [T_\varepsilon] \cdot [\varepsilon]_{x-y} \tag{A.12}$$

Then, comparing equation A.11 and A.12, the general transformation equation of stiffness matrix from material to laminate coordinate system is obtained, and can be written as:

$$[\overline{Q}] = [T_\sigma]^{-1} \cdot [Q] \cdot [T_\varepsilon] \tag{A.13}$$

A.3 Transformation of Stiffness Matrix for the Lamina that First Rotated θ about X-Axis, then β about Z-Axis

The stiffness matrix is first rotated an angle θ about x-axis. It can be written as:

$$[\overline{Q}] = [T_\sigma(\theta)]^{-1} \cdot [Q] \cdot [T_\varepsilon(\theta)] = [T_\sigma(-\theta)] \cdot [Q] \cdot [T_\varepsilon(\theta)]$$

$$\begin{bmatrix} \overline{Q}_{11} & \overline{Q}_{12} & \overline{Q}_{16} \\ \overline{Q}_{12} & \overline{Q}_{22} & \overline{Q}_{26} \\ \overline{Q}_{16} & \overline{Q}_{26} & \overline{Q}_{66} \end{bmatrix} = \begin{bmatrix} 1 & 0 & 0 \\ 0 & c_x^{\,2} & 0 \\ 0 & 0 & c_x \end{bmatrix} \cdot \begin{bmatrix} Q_{11} & Q_{12} & 0 \\ Q_{12} & Q_{22} & 0 \\ 0 & 0 & Q_{66} \end{bmatrix} \cdot \begin{bmatrix} 1 & 0 & 0 \\ 0 & c_x^{\,2} & 0 \\ 0 & 0 & c_x \end{bmatrix}$$

Thus,

$$\overline{Q}_{11} = Q_{11}$$

$$\overline{Q}_{12} = \overline{Q}_{21} = c_x^{\,2} Q_{12}$$

$$\overline{Q}_{22} = c_x^{\,4} Q \qquad \text{(A.14)}$$

$$\overline{Q}_{66} = c_x^{\,2} Q_{66}$$

$$\overline{Q}_{16} = \overline{Q}_{61} = \overline{Q}_{26} = \overline{Q}_{62} = 0$$

The transformed stiffness matrix $[\overline{Q}]$ is then rotated an angle β about z-axis. It can be expressed as:

$$[\hat{Q}] = [T_\sigma(\beta)]^{-1} \cdot [\overline{Q}] \cdot [T_\varepsilon(\beta)]$$

$$[\hat{Q}] = \begin{bmatrix} c_z^{\,2} & s_z^{\,2} & 2c_z s_z \\ s_z^{\,2} & c_z^{\,2} & -2c_z s_z \\ -c_z s_z & c_z s_z & c_z^{\,2} - s_z^{\,2} \end{bmatrix}^{-1} \cdot \begin{bmatrix} \overline{Q}_{11} & \overline{Q}_{12} & \overline{Q}_{16} \\ \overline{Q}_{12} & \overline{Q}_{22} & \overline{Q}_{26} \\ \overline{Q}_{16} & \overline{Q}_{26} & \overline{Q}_{66} \end{bmatrix} \cdot \begin{bmatrix} c_z^{\,2} & s_z^{\,2} & c_z s_z \\ s_z^{\,2} & c_z^{\,2} & -c_z s_z \\ -2c_z s_z & 2c_z s_z & c_z^{\,2} - s_z^{\,2} \end{bmatrix}$$

Thus,

$$\hat{Q}_{11} = c_z{}^4 Q_{11} + 2s_z{}^2 c_z{}^2 (c_x{}^2 Q_{12} + 2c_x{}^2 Q_{66}) + s_z{}^4 c_x{}^4 Q_{22}$$

$$\hat{Q}_{12} = s_z{}^2 c_z{}^2 (Q_{11} + c_x{}^4 Q_{22} - 4c_x{}^2 Q_{66}) + (s_z{}^4 + c_z{}^4) c_x{}^2 Q_{12}$$

$$\hat{Q}_{22} = s_z{}^4 Q_{11} + 2s_z{}^2 c_z{}^2 (c_x{}^2 Q_{12} + 2c_x{}^2 Q_{66}) + c_z{}^4 c_x{}^4 Q_{22}$$

$$\hat{Q}_{16} = s_z c_z{}^3 (Q_{11} - c_x{}^2 Q_{12} - 2c_x{}^2 Q_{66}) + s_z{}^3 c_z (c_x{}^2 Q_{12} - c_x{}^4 Q_{22} + 2c_x{}^2 Q_{66}) \quad \text{(A.15)}$$

$$\hat{Q}_{26} = s_z{}^3 c_z (Q_{11} - c_x{}^2 Q_{12} - 2c_x{}^2 Q_{66}) + s_z c_z{}^3 (c_x{}^2 Q_{12} - c_x{}^4 Q_{22} + 2c_x{}^2 Q_{66})$$

$$\hat{Q}_{66} = s_z{}^2 c_z{}^2 (Q_{11} + c_x{}^4 Q_{22} - 2c_x{}^2 Q_{12} - 2c_x{}^2 Q_{66}) + (s_z{}^4 + c_z{}^4) c_x{}^2 Q_{66}$$

A.4 Transformation of Coefficient of Thermal Expansion

$$[\alpha]_{x-y} = [T_\varepsilon]_z^{-1} \cdot [T_\varepsilon]_x^{-1} \cdot [\alpha]_{1-2}$$

$$\alpha_x = c_z{}^2 \alpha_1 + s_z{}^2 c_x{}^2 \alpha_2$$

$$\alpha_y = s_z{}^2 \alpha_1 + c_z{}^2 c_x{}^2 \alpha_2 \quad \text{(A.16)}$$

$$\alpha_{xy} = 2c_z s_z (\alpha_1 - c_x{}^2 \alpha_2)$$

A.5 Closed-Form Solution of Overall Thermal Induced Load of the Tubular Beam

$$\begin{aligned}
\overline{N}_x^T &= \int_0^{2\pi} N_x^T \cdot R \cdot d\theta \\
&= \int_0^{2\pi} \Delta T \cdot \sum_{k=1}^{n} (\hat{Q}_{11}^k \cdot \alpha_x^k + \hat{Q}_{12}^k \cdot \alpha_y^k + \hat{Q}_{16}^k \cdot \alpha_{xy}^k) \cdot (z_k^{'} - z_{k-1}^{'}) \cdot R \cdot d\theta \\
&= \pi \cdot R \cdot \Delta T \cdot \left\{ (c_z{}^6 + s_z{}^4 c_z{}^2 + 2 s_z{}^2 c_z{}^4)(2Q_{11}\alpha_1 + \frac{3}{4} Q_{12}\alpha_2) \right. \\
&\qquad \left. + (s_z{}^6 + s_z{}^2 c_z{}^4 + 2 s_z{}^4 c_z{}^2)(Q_{12}\alpha_1 + \frac{5}{8} Q_{22}\alpha_2) \right\} \cdot (z'_k - z'_{k-1}) \\
\overline{N}_y^T &= \int_0^{2\pi} N_y^T \cdot R \cdot d\theta \\
&= \int_0^{2\pi} \Delta T \cdot \sum_{k=1}^{n} (\hat{Q}_{12}^k \cdot \alpha_x^k + \hat{Q}_{22}^k \cdot \alpha_y^k + \hat{Q}_{26}^k \cdot \alpha_{xy}^k) \cdot (z_k^{'} - z_{k-1}^{'}) \cdot R \cdot d\theta \\
&= \pi \cdot R \cdot \Delta T \cdot \left\{ (s_z{}^6 + s_z{}^2 c_z{}^4 + 2 s_z{}^4 c_z{}^2)(2Q_{11}\alpha_1 + \frac{3}{4} Q_{12}\alpha_2) \right. \\
&\qquad \left. + (c_z{}^6 + s_z{}^4 c_z{}^2 + 2 s_z{}^2 c_z{}^4)(Q_{12}\alpha_1 + \frac{5}{8} Q_{22}\alpha_2) \right\} \cdot (z'_k - z'_{k-1}) \\
\overline{N}_{xy}^T &= \int_0^{2\pi} N_{xy}^T \cdot R \cdot d\theta \\
&= \int_0^{2\pi} \Delta T \cdot \sum_{k=1}^{n} (\hat{Q}_{16}^k \cdot \alpha_x^k + \hat{Q}_{26}^k \cdot \alpha_y^k + \hat{Q}_{66}^k \cdot \alpha_{xy}^k) \cdot (z_k^{'} - z_{k-1}^{'}) \cdot R \cdot d\theta \\
&= \pi \cdot R \cdot \Delta T \cdot \left\{ (s_z c_z{}^5 + s_z{}^5 c_z + 2 s_z{}^3 c_z{}^3) \right. \\
&\qquad \left. \cdot [(2Q_{11} - Q_{12})\alpha_1 + (\frac{3}{4} Q_{12} - \frac{5}{8} Q_{22})\alpha_2] \right\} \cdot (z'_k - z'_{k-1})
\end{aligned} \tag{A.17}$$

$$\overline{M}_x^T = \int_0^{2\pi} M_{xy}^T \cdot R \cdot d\theta = \int_0^{2\pi} (M_{x'}^T + R \cdot \cos\theta \cdot N_{x'}^T) \cdot R \cdot d\theta$$

$$= \int_0^{2\pi} \frac{\Delta T}{2} \cdot \sum_{k=1}^{n} (\hat{Q}_{11}^k \cdot \alpha_x^k + \hat{Q}_{12}^k \cdot \alpha_y^k + \hat{Q}_{16}^k \cdot \alpha_{xy}^k) \cdot (z_k^{'2} - z_{k-1}^{'2}) \cdot R \cdot d\theta$$

$$= \frac{\pi \cdot R \cdot \Delta T}{2} \cdot \left\{ (c_z^6 + s_z^4 c_z^2 + 2 s_z^2 c_z^4)(2Q_{11}\alpha_1 + \frac{3}{4} Q_{12}\alpha_2) \right.$$

$$\left. + (s_z^6 + s_z^2 c_z^4 + 2 s_z^4 c_z^2)(Q_{12}\alpha_1 + \frac{5}{8} Q_{22}\alpha_2) \right\} \cdot (z_k^{'2} - z_{k-1}^{'2})$$

$$\overline{M}_y^T = \int_0^{2\pi} M_y^T \cdot R \cdot d\theta = \int_0^{2\pi} (M_{y'}^T + R \cdot \cos\theta \cdot N_{y'}^T) \cdot R \cdot d\theta$$

$$= \int_0^{2\pi} \frac{\Delta T}{2} \cdot \sum_{k=1}^{n} (\hat{Q}_{12}^k \cdot \alpha_x^k + \hat{Q}_{22}^k \cdot \alpha_y^k + \hat{Q}_{26}^k \cdot \alpha_{xy}^k) \cdot (z_k^{'2} - z_{k-1}^{'2}) \cdot R \cdot d\theta \qquad \text{(A.18)}$$

$$= \frac{\pi \cdot R \cdot \Delta T}{2} \cdot \left\{ (s_z^6 + s_z^2 c_z^4 + 2 s_z^4 c_z^2)(2Q_{11}\alpha_1 + \frac{3}{4} Q_{12}\alpha_2) \right.$$

$$\left. + (c_z^6 + s_z^4 c_z^2 + 2 s_z^2 c_z^4)(Q_{12}\alpha_1 + \frac{5}{8} Q_{22}\alpha_2) \right\} \cdot (z_k^{'2} - z_{k-1}^{'2})$$

$$\overline{M}_{xy}^T = \int_0^{2\pi} M_{xy}^T \cdot R \cdot d\theta = \int_0^{2\pi} (M_{xy'}^T + R \cdot \cos\theta \cdot N_{xy'}^T) \cdot R \cdot d\theta$$

$$= \int_0^{2\pi} \frac{\Delta T}{2} \cdot \sum_{k=1}^{n} (\hat{Q}_{16}^k \cdot \alpha_x^k + \hat{Q}_{26}^k \cdot \alpha_y^k + \hat{Q}_{66}^k \cdot \alpha_{xy}^k) \cdot (z_k^{'2} - z_{k-1}^{'2}) \cdot R \cdot d\theta$$

$$= \frac{\pi \cdot R \cdot \Delta T}{2} \cdot \left\{ (s_z c_z^5 + s_z^5 c_z + 2 s_z^3 c_z^3) \right.$$

$$\left. \cdot [(2Q_{11} - Q_{12})\alpha_1 + (\frac{3}{4} Q_{12} - \frac{5}{8} Q_{22})\alpha_2] \right\} \cdot (z_k^{'2} - z_{k-1}^{'2})$$

Where $c_z = \cos\beta$ and $s_z = \sin\beta$.

APPENDIX B

MATLAB CODES FOR ANALYTICAL SOLUTIONS

B.1 Main Program for Rectangular Beam

```
clear all
close all
clc
global angle nply tply q Q11 Q12 Q22 Q66 k abd a1 a2

%~~~~~~~~~~~~~~~~~~~~~~~~~~~~~~~~~~~~~~~~~~~~~~~~~~~~~~~~~~~~~~~~~~~~~~~~~~~~
% Define the Input Variables
%~~~~~~~~~~~~~~~~~~~~~~~~~~~~~~~~~~~~~~~~~~~~~~~~~~~~~~~~~~~~~~~~~~~~~~~~~~~~
syms theta
angle=[0 0 -45 45 90 90 -45 45 0 0 -45 45 90 90 -45 45]*(pi/180);
nply=16;
tply=0.005;
q=1;
delT=0;

%~~~~~~~~~~~~~~~~~~~~~~~~~~~~~~~~~~~~~~~~~~~~~~~~~~~~~~~~~~~~~~~~~~~~~~~~~~~~
% Define Material Properties
%~~~~~~~~~~~~~~~~~~~~~~~~~~~~~~~~~~~~~~~~~~~~~~~~~~~~~~~~~~~~~~~~~~~~~~~~~~~~
E1=21.3E6;
E2=1.5E6;
v12=0.27;
G12=1.0E6;
a1=-0.5E-6;
a2=15E-6;

%~~~~~~~~~~~~~~~~~~~~~~~~~~~~~~~~~~~~~~~~~~~~~~~~~~~~~~~~~~~~~~~~~~~~~~~~~~~~
% Calculation of Q Matrix
%~~~~~~~~~~~~~~~~~~~~~~~~~~~~~~~~~~~~~~~~~~~~~~~~~~~~~~~~~~~~~~~~~~~~~~~~~~~~
v21=(v12*E2)/E1;
Q11=E1/(1-v12*v21);
Q12=(v12*E2)/(1-v12*v21);
Q22=E2/(1-v12*v21);
Q66=G12;

%~~~~~~~~~~~~~~~~~~~~~~~~~~~~~~~~~~~~~~~~~~~~~~~~~~~~~~~~~~~~~~~~~~~~~~~~~~~~
% Calculation of A Matrix
%~~~~~~~~~~~~~~~~~~~~~~~~~~~~~~~~~~~~~~~~~~~~~~~~~~~~~~~~~~~~~~~~~~~~~~~~~~~~
A11=0;
A12=0;
A16=0;
A22=0;
```

```
A26=0;
A66=0;

for k=1:nply
    A11=A11+Qb11(k)*(h(k)-h(k-1));
end
for k=1:nply
    A12=A12+Qb12(k)*(h(k)-h(k-1));
end
for k=1:nply
    A16=A16+Qb16(k)*(h(k)-h(k-1));
end
for k=1:nply
    A22=A22+Qb22(k)*(h(k)-h(k-1));
end
for k=1:nply
    A26=A26+Qb26(k)*(h(k)-h(k-1));
end
for k=1:nply
    A66=A66+Qb66(k)*(h(k)-h(k-1));
end

A=[A11 A12 A16;
     A12 A22 A26;
     A16 A26 A66];

%~~~~~~~~~~~~~~~~~~~~~~~~~~~~~~~~~~~~~~~~~~~~~~~~~~~~~~~~~~~~~~~~~~~~~~~~~~~~
% Calculation of B Matrix
%~~~~~~~~~~~~~~~~~~~~~~~~~~~~~~~~~~~~~~~~~~~~~~~~~~~~~~~~~~~~~~~~~~~~~~~~~~~~
B11=0;
B12=0;
B16=0;
B22=0;
B26=0;
B66=0;

for k=1:nply
   B11=B11+(1/2)*Qb11(k)*(h(k)^2-h(k-1)^2);
end
for k=1:nply
    B12=B12+(1/2)*Qb12(k)*(h(k)^2-h(k-1)^2);
end
for k=1:nply
    B16=B16+(1/2)*Qb16(k)*(h(k)^2-h(k-1)^2);
```

```
end
for k=1:nply
    B22=B22+(1/2)*Qb22(k)*(h(k)^2-h(k-1)^2);
end
for k=1:nply
    B26=B26+(1/2)*Qb26(k)*(h(k)^2-h(k-1)^2);
end
for k=1:nply
    B66=B66+(1/2)*Qb66(k)*(h(k)^2-h(k-1)^2);
end

B=[B11 B12 B16;
     B12 B22 B26;
     B16 B26 B66];

%~~~~~~~~~~~~~~~~~~~~~~~~~~~~~~~~~~~~~~~~~~~~~~~~~~~~~~~~~~~~~~~~~~~~~~~~~~~~
% Calculation of D Matrix
%~~~~~~~~~~~~~~~~~~~~~~~~~~~~~~~~~~~~~~~~~~~~~~~~~~~~~~~~~~~~~~~~~~~~~~~~~~~~
D11=0;
D12=0;
D16=0;
D22=0;
D26=0;
D66=0;

for k=1:nply
    D11=D11+(1/3)*Qb11(k)*(h(k)^3-h(k-1)^3);
end
for k=1:nply
    D12=D12+(1/3)*Qb12(k)*(h(k)^3-h(k-1)^3);
end
for k=1:nply
    D16=D16+(1/3)*Qb16(k)*(h(k)^3-h(k-1)^3);
end
for k=1:nply
    D22=D22+(1/3)*Qb22(k)*(h(k)^3-h(k-1)^3);
end
for k=1:nply
    D26=D26+(1/3)*Qb26(k)*(h(k)^3-h(k-1)^3);
end
for k=1:nply
    D66=D66+(1/3)*Qb66(k)*(h(k)^3-h(k-1)^3);
end
```

```
D=[D11 D12 D16;
    D12 D22 D26;
    D16 D26 D66];

%~~~~~~~~~~~~~~~~~~~~~~~~~~~~~~~~~~~~~~~~~~~~~~~~~~~~~~~~~~~~~~~~~~~~~~~~~~~~
% Calculation of Thermal Induced loads and Moments
%~~~~~~~~~~~~~~~~~~~~~~~~~~~~~~~~~~~~~~~~~~~~~~~~~~~~~~~~~~~~~~~~~~~~~~~~~~~~
NTx=0;
NTy=0;
NTxy=0;
MTx=0;
MTy=0;
MTxy=0;

for k=1:nply
   NTx=NTx+(delT*(h(k)-h(k-1))*(Qb11(k)*alphax(k)+Qb12(k)*alphay(k)
          +Qb16(k)*alphaxy(k)));
end
for k=1:nply
   NTy=NTy+delT*(h(k)-h(k-1))*(Qb12(k)*alphax(k)+Qb22(k)*alphay(k)
          +Qb26(k)*alphaxy(k));
end
for k=1:nply
   NTxy=NTxy+delT*(h(k)-h(k-1))*(Qb16(k)*alphax(k)+Qb26(k)*alphay(k)
          +Qb66(k)*alphaxy(k));
end

for k=1:nply
   MTx=MTx+((1/2)*delT*((h(k))^2-(h(k-1))^2)*(Qb11(k)*alphax(k)
          +Qb12(k)*alphay(k)+Qb16(k)*alphaxy(k)));
end
for k=1:nply
   MTy=MTy+((1/2)*delT*((h(k))^2-(h(k-1))^2)*(Qb12(k)*alphax(k)
          +Qb22(k)*alphay(k)+Qb26(k)*alphaxy(k)));
end
for k=1:nply
   MTxy=MTxy+((1/2)*delT*((h(k))^2-(h(k1))^2)*(Qb16(k)*alphax(k)
           +Qb26(k)*alphay(k)+Qb66(k)*alphaxy(k)));
end

%~~~~~~~~~~~~~~~~~~~~~~~~~~~~~~~~~~~~~~~~~~~~~~~~~~~~~~~~~~~~~~~~~~~~~~~~~~~~
% Calculation of Mid-Plane Strain and Curvature
%~~~~~~~~~~~~~~~~~~~~~~~~~~~~~~~~~~~~~~~~~~~~~~~~~~~~~~~~~~~~~~~~~~~~~~~~~~~~
ABD=[A B; B D];
```

```
abd=inv(ABD);
a=[abd(1,1) abd(1,2) abd(1,3);
    abd(2,1) abd(2,2) abd(2,3);
    abd(3,1) abd(3,2) abd(3,3)];
b=[abd(1,4) abd(1,5) abd(1,6);
     abd(2,4) abd(2,5) abd(2,6);
     abd(3,4) abd(3,5) abd(3,6)];
bt=[abd(4,1) abd(4,2) abd(4,3);
      abd(5,1) abd(5,2) abd(5,3);
      abd(6,1) abd(6,2) abd(6,3)];
d=[abd(4,4) abd(4,5) abd(4,6);
    abd(5,4) abd(5,5) abd(5,6);
    abd(6,4) abd(6,5) abd(6,6)];

NM=[0; 0; 0; -5; 0; 0];
NTMT=[NTx; NTy; NTxy; MTx; MTy; MTxy];
NMb=NM+NTMT;

E0K=abd*NMb
E0=[E0K(1,1); E0K(2,1); E0K(3,1)];
K=[E0K(4,1); E0K(5,1); E0K(6,1)];

%~~~~~~~~~~~~~~~~~~~~~~~~~~~~~~~~~~~~~~~~~~~~~~~~~~~~~~~~~~~~~~~~~~~~~~~~~~~
% Calculation of In-Plane Stresses
%~~~~~~~~~~~~~~~~~~~~~~~~~~~~~~~~~~~~~~~~~~~~~~~~~~~~~~~~~~~~~~~~~~~~~~~~~~~
for k=1:nply
   stress=([Qb11(k) Qb12(k) Qb16(k); Qb12(k) Qb22(k) Qb26(k); Qb16(k) Qb26(k)
            Qb66(k)]*((E0+h(k)*K)-delT*[alphax(k); alphay(k); alphaxy(k)])+[Qb11(k)
            Qb12(k) Qb16(k); Qb12(k) Qb22(k) Qb26(k); Qb16(k) Qb26(k)
            Qb66(k)]*((E0+h(k-1)*K)-delT*[alphax(k); alphay(k); alphaxy(k)]))/2
end

%~~~~~~~~~~~~~~~~~~~~~~~~~~~~~~~~~~~~~~~~~~~~~~~~~~~~~~~~~~~~~~~~~~~~~~~~~~~
% Calculation of Interlaminar Shear Stresses
%~~~~~~~~~~~~~~~~~~~~~~~~~~~~~~~~~~~~~~~~~~~~~~~~~~~~~~~~~~~~~~~~~~~~~~~~~~~
Tfirst=0;
Tsecond=0;
for k=1:nply
   Tfirst=Tfirst+QBb(k)*(h(k)-h(k-1));
   Tsecond=Tsecond+(1/2)*(QDb(k)*(h(k)^2-h(k-1)^2));
   Txz(:,:,k)=-q*(Tfirst+Tsecond);
end
```

B.2 Main Program for Circular Tube

```
clear all
close all
clc
syms theta
global angle nply tply R Q11 Q12 Q22 Q66 k a1 a2

%~~~~~~~~~~~~~~~~~~~~~~~~~~~~~~~~~~~~~~~~~~~~~~~~~~~~~~~~~~~~~~~~~~~~~~~~
% Define the Input Variables
%~~~~~~~~~~~~~~~~~~~~~~~~~~~~~~~~~~~~~~~~~~~~~~~~~~~~~~~~~~~~~~~~~~~~~~~~
angle=[45 -45 90 0 90 0 45 -45 -45 45 0 90 0 90 -45 45]*(pi/180);
nply=16;
tply=0.005;
R=1;
delT=50;
length=10;

%~~~~~~~~~~~~~~~~~~~~~~~~~~~~~~~~~~~~~~~~~~~~~~~~~~~~~~~~~~~~~~~~~~~~~~~~
% Define Material Properties
%~~~~~~~~~~~~~~~~~~~~~~~~~~~~~~~~~~~~~~~~~~~~~~~~~~~~~~~~~~~~~~~~~~~~~~~~
E1=21.3E6;
E2=1.5E6;
v12=0.27;
G12=1.0E6;
a1=-0.5E-6;
a2=15E-6;

%~~~~~~~~~~~~~~~~~~~~~~~~~~~~~~~~~~~~~~~~~~~~~~~~~~~~~~~~~~~~~~~~~~~~~~~~
% Calculation of Q Matrix
%~~~~~~~~~~~~~~~~~~~~~~~~~~~~~~~~~~~~~~~~~~~~~~~~~~~~~~~~~~~~~~~~~~~~~~~~
v21=(v12*E2)/E1;
Q11=E1/(1-v12*v21);
Q12=(v12*E2)/(1-v12*v21);
Q22=E2/(1-v12*v21);
Q66=G12;

%~~~~~~~~~~~~~~~~~~~~~~~~~~~~~~~~~~~~~~~~~~~~~~~~~~~~~~~~~~~~~~~~~~~~~~~~
% Calculation of A-Bar Matrix
%~~~~~~~~~~~~~~~~~~~~~~~~~~~~~~~~~~~~~~~~~~~~~~~~~~~~~~~~~~~~~~~~~~~~~~~~
A11=0;
A12=0;
A16=0;
```

```
A22=0;
A26=0;
A66=0;

for k=1:nply
   A11=A11+R*(h(k)-h(k-1))*(quad('Qh11',0,2*pi));
end
for k=1:nply
   A12=A12+R*(h(k)-h(k-1))*(quad('Qh12',0,2*pi));
end
for k=1:nply
   A16=A16+R*(h(k)-h(k-1))*(quad('Qh16',0,2*pi));
end
for k=1:nply
   A22=A22+R*(h(k)-h(k-1))*(quad('Qh22',0,2*pi));
end
for k=1:nply
   A26=A26+R*(h(k)-h(k-1))*(quad('Qh26',0,2*pi));
end
for k=1:nply
   A66=A66+R*(h(k)-h(k-1))*(quad('Qh66',0,2*pi));
end

A=[A11 A12 A16;
     A12 A22 A26;
     A16 A26 A66];

%~~~~~~~~~~~~~~~~~~~~~~~~~~~~~~~~~~~~~~~~~~~~~~~~~~~~~~~~~~~~~~~~~~~~~~~~~~~~
% Calculation of B-Bar Matrix
%~~~~~~~~~~~~~~~~~~~~~~~~~~~~~~~~~~~~~~~~~~~~~~~~~~~~~~~~~~~~~~~~~~~~~~~~~~~~
B11=0;
B12=0;
B16=0;
B22=0;
B26=0;
B66=0;

for k=1:nply
   B11=B11+(R/2)*(h(k)^2-h(k-1)^2)*(quad('Qh11',0,2*pi))+(R^2)*(h(k)-h(k-1))
         *(quad('cQh11',0,2*pi));
end
for k=1:nply
   B12=B12+(R/2)*(h(k)^2-h(k-1)^2)*(quad('Qh12',0,2*pi))+(R^2)*(h(k)-h(k-1))
         *(quad('cQh12',0,2*pi));
```

```
end
for k=1:nply
   B16=B16+(R/2)*(h(k)^2-h(k-1)^2)*(quad('Qh16',0,2*pi))+(R^2)*(h(k)-h(k-1))
         *(quad('cQh16',0,2*pi));
end
for k=1:nply
   B22=B22+(R/2)*(h(k)^2-h(k-1)^2)*(quad('Qh22',0,2*pi))+(R^2)*(h(k)-h(k-1))
         *(quad('cQh22',0,2*pi));
end
for k=1:nply
   B26=B26+(R/2)*(h(k)^2-h(k-1)^2)*(quad('Qh26',0,2*pi))+(R^2)*(h(k)-h(k-1))
         *(quad('cQh26',0,2*pi));
end
for k=1:nply
   B66=B66+(R/2)*(h(k)^2-h(k-1)^2)*(quad('Qh66',0,2*pi))+(R^2)*(h(k)-h(k-1))
         *(quad('cQh66',0,2*pi));
end

B=[B11 B12 B16;
    B12 B22 B26;
    B16 B26 B66];

%~~~~~~~~~~~~~~~~~~~~~~~~~~~~~~~~~~~~~~~~~~~~~~~~~~~~~~~~~~~~~~~~~~~~~~~~
% Calculation of D-Bar Matrix
%~~~~~~~~~~~~~~~~~~~~~~~~~~~~~~~~~~~~~~~~~~~~~~~~~~~~~~~~~~~~~~~~~~~~~~~~
D11=0;
D12=0;
D16=0;
D22=0;
D26=0;
D66=0;


for k=1:nply
   D11=D11+(R/3)*(h(k)^3-h(k-1)^3)*(quad('Qh11',0,2*pi))+(R^2)*(h(k)^2-h(k-1)^2)
         *(quad('cQh11',0,2*pi))+(R^3)*(h(k)-h(k-1))*(quad('ccQh11',0,2*pi));
end
for k=1:nply
   D12=D12+(R/3)*(h(k)^3-h(k-1)^3)*(quad('Qh12',0,2*pi))+(R^2)*(h(k)^2-h(k-1)^2)
         *(quad('cQh12',0,2*pi))+(R^3)*(h(k)-h(k-1))*(quad('ccQh12',0,2*pi));
end
for k=1:nply
   D16=D16+(R/3)*(h(k)^3-h(k-1)^3)*(quad('Qh16',0,2*pi))+(R^2)*(h(k)^2-h(k-1)^2)
         *(quad('cQh16',0,2*pi))+(R^3)*(h(k)-h(k-1))*(quad('ccQh16',0,2*pi));
```

```
end
for k=1:nply
   D22=D22+(R/3)*(h(k)^3-h(k-1)^3)*(quad('Qh22',0,2*pi))+(R^2)*(h(k)^2-h(k-1)^2)
         *(quad('cQh22',0,2*pi))+(R^3)*(h(k)-h(k-1))*(quad('ccQh22',0,2*pi));
end
for k=1:nply
   D26=D26+(R/3)*(h(k)^3-h(k-1)^3)*(quad('Qh26',0,2*pi))+(R^2)*(h(k)^2-h(k-1)^2)
         *(quad('cQh26',0,2*pi))+(R^3)*(h(k)-h(k-1))*(quad('ccQh26',0,2*pi));
end;
for k=1:nply
   D66=D66+(R/3)*(h(k)^3-h(k-1)^3)*(quad('Qh66',0,2*pi))+(R^2)*(h(k)^2-h(k-1)^2)
         *(quad('cQh66',0,2*pi))+(R^3)*(h(k)-h(k-1))*(quad('ccQh66',0,2*pi));
end

D=[D11 D12 D16;
    D12 D22 D26;
    D16 D26 D66];

ABD=[A B;
        B D];

NM=[0; 0; 0; 50; 0; 0];

%~~~~~~~~~~~~~~~~~~~~~~~~~~~~~~~~~~~~~~~~~~~~~~~~~~~~~~~~~~~~~~~~~~~~~~~~~~~
% Calculation of Thermal Induced loads and Moments
%~~~~~~~~~~~~~~~~~~~~~~~~~~~~~~~~~~~~~~~~~~~~~~~~~~~~~~~~~~~~~~~~~~~~~~~~~~~
NTxp=0;
NTyp=0;
NTxyp=0;
MTxp=0;
MTyp=0;
MTxyp=0;

for k=1:nply
   NTxp=NTxp+delT*(h(k)-h(k-1))*(Qh11(theta)*alphax(theta)
         +Qh12(theta)*alphay(theta)+Qh16(theta)*alphaxy(theta));
end
for k=1:nply
   NTyp=NTyp+delT*(h(k)-h(k-1))*(Qh12(theta)*alphax1(theta)
          +Qh22(theta)*alphay1(theta)+Qh26(theta)*alphaxy1(theta));
end
for k=1:nply
   NTxyp=NTxyp+delT*(h(k)-h(k-1))*(Qh16(theta)*alphax(theta)
          +Qh26(theta)*alphay(theta)+Qh66(theta)*alphaxy(theta));
```

```
end

for k=1:nply
   MTxp=MTxp+(1/2)*delT*((h(k))^2-(h(k-1))^2)*(Qh11(theta)*alphax(theta)
            +Qh12(theta)*alphay(theta)+Qh16(theta)*alphaxy(theta));
end
for k=1:nply
   MTyp=MTyp+(1/2)*delT*((h(k))^2-(h(k-1))^2)*(Qh12(theta)*alphax1(theta)
            +Qh22(theta)*alphay1(theta)+Qh26(theta)*alphaxy1(theta));
end
for k=1:nply
   MTxyp=MTxyp+(1/2)*delT*((h(k))^2-(h(k-1))^2)*(Qh16(theta)*alphax(theta)
             +Qh26(theta)*alphay(theta)+Qh66(theta)*alphaxy(theta));
end

NTx=NTxp;
NTy=NTyp;
NTxy=NTxyp;
MTx=MTxp+R*cos(theta)*NTxp;
MTy=MTyp+R*cos(theta)*NTyp;
MTxy=MTxyp+R*cos(theta)*NTxyp;

NTxb=int(NTx*R,theta,0,2*pi);
NTyb=int(NTy*R,theta,0,2*pi);
NTxyb=int(NTxy*R,theta,0,2*pi);

MTxb=int(MTx*R,theta,0,2*pi);
MTyb=int(MTy*R,theta,0,2*pi);
MTxyb=int(MTxy*R,theta,0,2*pi);

NTb=[NTxb; NTyb; NTxyb];

MTb=[MTxb; MTyb; MTxyb];

NMTb=[NTb; MTb];
NMb=NM+NMTb;

%~~~~~~~~~~~~~~~~~~~~~~~~~~~~~~~~~~~~~~~~~~~~~~~~~~~~~~~~~~~~~~~~~~~~~~~~
% Calculation of Mid-Plane Strain and Curvature
%~~~~~~~~~~~~~~~~~~~~~~~~~~~~~~~~~~~~~~~~~~~~~~~~~~~~~~~~~~~~~~~~~~~~~~~~
midstrain=vpa(inv(ABD)*NMb,5)

E0=[midstrain(1,1); midstrain(2,1); midstrain(3,1)];
K=[midstrain(4,1); midstrain(5,1); midstrain(6,1)];
```

```
function y=h(x)
global nply tply
y=-(nply/2)*tply+x*tply;

function y = Qb11(x)
global angle Q11 Q12 Q22 Q66 k
y=cos(angle(k)).^4*Q11+sin(angle(k)).^4*Q22+2*(Q12+2*Q66)*cos(angle(k)).^2
   *sin(angle(k)).^2;

function y = Qb12(x)
global angle Q11 Q12 Q22 Q66 k
y=cos(angle(k)).^2*sin(angle(k)).^2*(Q11+Q22-4*Q66)+(cos(angle(k)).^4
   +sin(angle(k)).^4)*Q12;

function y = Qb16(x)
global angle Q11 Q12 Q22 Q66 k
y=cos(angle(k)).^3*sin(angle(k))*(Q11-Q12-2*Q66)-cos(angle(k))*sin(angle(k)).^3
   *(Q22-Q12-2*Q66);

function y = Qb22(x)
global angle Q11 Q12 Q22 Q66 k
y=sin(angle(k)).^4*Q11+cos(angle(k)).^4*Q22+2*(Q12+2*Q66)*cos(angle(k)).^2
   *sin(angle(k)).^2;

function y = Qb26(x)
global angle Q11 Q12 Q22 Q66 k
y=cos(angle(k))*sin(angle(k)).^3*(Q11-Q12-2*Q66)-cos(angle(k)).^3*sin(angle(k))
   *(Q22-Q12-2*Q66);

function y = Qb66(x)
global angle Q11 Q12 Q22 Q66 k
y=cos(angle(k)).^2*sin(angle(k)).^2*(Q11+Q22-2*Q12-2*Q66)+(cos(angle(k)).^4
   +sin(angle(k)).^4)*Q66;

function y = QBb(x)
global angle Q11 Q12 Q22 Q66 k abd
y=Qb11(k)*abd(1,4)+Qb12(k)*abd(2,4)+Qb16(k)*abd(3,4);

function y = QDb(x)
global angle Q11 Q12 Q22 Q66 k abd
y=Qb11(k)*abd(4,4)+Qb12(k)*abd(5,4)+Qb16(k)*abd(6,4);
```

```
function y = alphax(x)
global angle a1 a2 k
y=a1*cos(-angle(k))^2+a2*sin(-angle(k))^2*cos(-x)^2;

function y = alphay(x)
global angle a1 a2 k
y=a1*sin(-angle(k))^2+a2*cos(-angle(k))^2*cos(-x)^2;

function y = alphaxy(x)
global angle a1 a2 k
y=-2*a1*cos(-angle(k))*sin(-angle(k))+2*a2*cos(-angle(k))*sin(-angle(k))*cos(-x)^2;

function y = CTExy(x)
global angle a1 a2 k
y=[alphax(x); alphay(x); alphaxy(x)];

function y = Qh11(x)
global angle Q11 Q12 Q22 Q66 k
y=cos(angle(k)).^4*Q11+sin(angle(k)).^4*cos(x).^4*Q22+2*cos(angle(k)).^2
   *sin(angle(k)).^2*cos(x).^2*Q12+4*cos(angle(k)).^2*sin(angle(k)).^2*cos(x).^2
   *Q66;

function y = Qh12(x)
global angle Q11 Q12 Q22 Q66 k
y=cos(angle(k)).^2*sin(angle(k)).^2*Q11+cos(angle(k)).^2*sin(angle(k)).^2*cos(x).^4
   *Q22+(cos(angle(k)).^4+sin(angle(k)).^4)*cos(x).^2*Q12-4*cos(angle(k)).^2
   *sin(angle(k)).^2*cos(x).^2*Q66;

function y = Qh16(x)
global angle Q11 Q12 Q22 Q66 k
y=cos(angle(k)).^3*sin(angle(k))*Q11-cos(angle(k))*sin(angle(k)).^3*cos(x).^4
   *Q22+(cos(angle(k))*sin(angle(k)).^3-cos(angle(k)).^3*sin(angle(k)))*cos(x).^2
   *Q12+2*(cos(angle(k))*sin(angle(k)).^3-cos(angle(k)).^3*sin(angle(k)))*cos(x).^2
   *Q66;

function y = Qh22(x)
global angle Q11 Q12 Q22 Q66 k
y=sin(angle(k)).^4*Q11+cos(angle(k)).^4*cos(x).^4*Q22+2*cos(angle(k)).^2
   *sin(angle(k)).^2*cos(x).^2*Q12+4*cos(angle(k)).^2*sin(angle(k)).^2*cos(x).^2
   *Q66;
function y = Qh26(x)
global angle Q11 Q12 Q22 Q66 k
```

```
y=cos(angle(k))*sin(angle(k)).^3*Q11-cos(angle(k)).^3*sin(angle(k))*cos(x).^4
   *Q22+(cos(angle(k)).^3*sin(angle(k))-cos(angle(k))*sin(angle(k)).^3)*cos(x).^2
   *Q12+2*(cos(angle(k)).^3*sin(angle(k))-cos(angle(k))*sin(angle(k)).^3)*cos(x).^2
   *Q66;

function y = Qh66(x)
global angle Q11 Q12 Q22 Q66 k
y=cos(angle(k)).^2*sin(angle(k)).^2*Q11+cos(angle(k)).^2*sin(angle(k)).^2*cos(x).^4
   *Q22-2*cos(angle(k)).^2*sin(angle(k)).^2*cos(x).^2*Q12+(cos(angle(k)).^2
   +sin(angle(k)).^2).^2*cos(x).^2*Q66;

function y = cQh11(x)
global angle Q11 Q12 Q22 Q66 k
y=Qh11(x).*cos(x);

function y = cQh12(x)
global angle Q11 Q12 Q22 Q66 k
y=Qh12(x).*cos(x);

function y = cQh16(x)
global angle Q11 Q12 Q22 Q66 k
y=Qh16(x).*cos(x);

function y = cQh22(x)
global angle Q11 Q12 Q22 Q66 k
y=Qh22(x).*cos(x);

function y = cQh26(x)
global angle Q11 Q12 Q22 Q66 k
y=Qh26(x).*cos(x);
function y = cQh66(x)
global angle Q11 Q12 Q22 Q66 k
y=Qh66(x).*cos(x);

function y = ccQh11(x)
global angle Q11 Q12 Q22 Q66 k
y=Qh11(x).*cos(x).^2;

function y = ccQh12(x)
global angle Q11 Q12 Q22 Q66 k
y=Qh12(x).*cos(x).^2;

function y = ccQh16(x)
global angle Q11 Q12 Q22 Q66 k
```

```
y=Qh16(x).*cos(x).^2;

function y = ccQh22(x)
global angle Q11 Q12 Q22 Q66 k
y=Qh22(x).*cos(x).^2;

function y = ccQh26(x)
global angle Q11 Q12 Q22 Q66 k
y=Qh26(x).*cos(x).^2;

function y = ccQh66(x)
global angle Q11 Q12 Q22 Q66 k
y=Qh66(x).*cos(x).^2;
```

APPENDIX C

ANSYS 10 BATCH CODES FOR FINITE ELEMENT MODELS

C.1 Ansys 10 Batch Code for Rectangular Beam

```
/FILNAM, Composite beam
/TITLE, Composite Beam

/UNITS,BIN
/PREP7

!~~~~~~~~~~~~~~~~~~~~~~~~~~~~~~~~~~~~~~~~~~~~~~~~~~~~~~~~~~~~~~~~~~~~
! Define the input varianles
!~~~~~~~~~~~~~~~~~~~~~~~~~~~~~~~~~~~~~~~~~~~~~~~~~~~~~~~~~~~~~~~~~~~~

width=0.5
length=10
tply=0.005

!~~~~~~~~~~~~~~~~~~~~~~~~~~~~~~~~~~~~~~~~~~~~~~~~~~~~~~~~~~~~~~~~~~~~
! Define Material Properties
!~~~~~~~~~~~~~~~~~~~~~~~~~~~~~~~~~~~~~~~~~~~~~~~~~~~~~~~~~~~~~~~~~~~~

!Carbon/Epoxy AS4/3501-6

MP,EX,1,21.3E6
MP,EY,1,1.5E6
MP,EZ,1,1.5E6
MP,PRXY,1,0.27
MP,PRXZ,1,0.27
MP,PRYZ,1,0.27
MP,GXY,1,1.0E6
MP,GXZ,1,1.0E6
MP,GYZ,1,1.0E6
MP,ALPX,1,-0.5E-6
MP,ALPY,1,15E-6
MP,ALPZ,1,15E-6

!~~~~~~~~~~~~~~~~~~~~~~~~~~~~~~~~~~~~~~~~~~~~~~~~~~~~~~~~~~~~~~~~~~~~
! Define Element Type and Real Constants
!~~~~~~~~~~~~~~~~~~~~~~~~~~~~~~~~~~~~~~~~~~~~~~~~~~~~~~~~~~~~~~~~~~~~

ET,1,SOLID46

R,1
RMODIF,1,1,1,0,0,0,0
```

```
RMODIF,1,7,0
RMODIF,1,13,1,45,tply

R,2
RMODIF,2,1,1,0,0,0,0
RMODIF,2,7,0
RMODIF,2,13,1,-45,tply

R,3
RMODIF,3,1,1,0,0,0,0
RMODIF,3,7,0
RMODIF,3,13,1,90,tply

R,4
RMODIF,4,1,1,0,0,0,0
RMODIF,4,7,0
RMODIF,4,13,1,0,tply

R,5
RMODIF,5,1,1,0,0,0,0
RMODIF,5,7,0
RMODIF,5,13,1,90,tply

R,6
RMODIF,6,1,1,0,0,0,0
RMODIF,6,7,0
RMODIF,6,13,1,0,tply

R,7
RMODIF,7,1,1,0,0,0,0
RMODIF,7,7,0
RMODIF,7,13,1,45,tply

R,8
RMODIF,8,1,1,0,0,0,0
RMODIF,8,7,0
RMODIF,8,13,1,-45,tply

R,9
RMODIF,9,1,1,0,0,0,0
RMODIF,9,7,0
RMODIF,9,13,1,-45,tply

R,10
```

```
RMODIF,10,1,1,0,0,0,0
RMODIF,10,7,0
RMODIF,10,13,1,45,tply

R,11
RMODIF,11,1,1,0,0,0,0
RMODIF,11,7,0
RMODIF,11,13,1,0,tply

R,12
RMODIF,12,1,1,0,0,0,0
RMODIF,12,7,0
RMODIF,12,13,1,90,tply

R,13
RMODIF,13,1,1,0,0,0,0
RMODIF,13,7,0
RMODIF,13,13,1,0,tply

R,14
RMODIF,14,1,1,0,0,0,0
RMODIF,14,7,0
RMODIF,14,13,1,90,tply

R,15
RMODIF,15,1,1,0,0,0,0
RMODIF,15,7,0
RMODIF,15,13,1,-45,tply

R,16
RMODIF,16,1,1,0,0,0,0
RMODIF,16,7,0
RMODIF,16,13,1,45,tply

!~~~~~~~~~~~~~~~~~~~~~~~~~~~~~~~~~~~~~~~~~~~~~~~~~~~~~~~~~~~~~~~~~~~~~~~
! Define the Geometry of the Beam
!~~~~~~~~~~~~~~~~~~~~~~~~~~~~~~~~~~~~~~~~~~~~~~~~~~~~~~~~~~~~~~~~~~~~~~~

*DO,I,1,16,1
K,1+4*(I-1),0,-width/2,tply*(I-1)
K,2+4*(I-1),0,width/2,tply*(I-1)
K,3+4*(I-1),length,width/2,tply*(I-1)
K,4+4*(I-1),length,-width/2,tply*(I-1)
A,1+4*(I-1),2+4*(I-1),3+4*(I-1),4+4*(I-1)
```

```
*ENDDO

*DO,K,1,16,1
VOFFST,K,-tply
*ENDDO

NUMMRG,KP,1.0e-4

!~~~~~~~~~~~~~~~~~~~~~~~~~~~~~~~~~~~~~~~~~~~~~~~~~~~~~~~~~~~~~~~~~~~~~~~
! Define number of the Element on Each Line
!~~~~~~~~~~~~~~~~~~~~~~~~~~~~~~~~~~~~~~~~~~~~~~~~~~~~~~~~~~~~~~~~~~~~~~~

ALLSEL
LSEL,S,LENGTH,,width
lplot
LESIZE,ALL,,,10

ALLSEL
LSEL,S,LENGTH,,10
lplot
LESIZE,ALL,,,50

ALLSEL
LSEL,S,LENGTH,,tply
lplot
LESIZE,ALL,,,1

!~~~~~~~~~~~~~~~~~~~~~~~~~~~~~~~~~~~~~~~~~~~~~~~~~~~~~~~~~~~~~~~~~~~~~~~
! Mesh the Volumes
!~~~~~~~~~~~~~~~~~~~~~~~~~~~~~~~~~~~~~~~~~~~~~~~~~~~~~~~~~~~~~~~~~~~~~~~

*DO,I,1,16,1
ALLSEL
TYPE,1,
ESYS,0
MAT,1,
REAL,16-(I-1)
VMESH,I
*ENDDO
EPLOT

!~~~~~~~~~~~~~~~~~~~~~~~~~~~~~~~~~~~~~~~~~~~~~~~~~~~~~~~~~~~~~~~~~~~~~~~
! Merge All Coincident Nedes,Elements, and Key points
!~~~~~~~~~~~~~~~~~~~~~~~~~~~~~~~~~~~~~~~~~~~~~~~~~~~~~~~~~~~~~~~~~~~~~~~
```

```
ALLSEL
NUMMRG,NODE,1.0e-4
NUMMRG,ELEM,1.0e-4
NUMMRG,KP,1.0e-4
EPLOT

CSYS,0

!~~~~~~~~~~~~~~~~~~~~~~~~~~~~~~~~~~~~~~~~~~~~~~~~~~~~~~~~~~~~~~~~~~~~~~~~
! Apply Constraints, Load, and Temperature Change
!~~~~~~~~~~~~~~~~~~~~~~~~~~~~~~~~~~~~~~~~~~~~~~~~~~~~~~~~~~~~~~~~~~~~~~~~

ALLSEL
NSEL,S,LOC,X,0
D,ALL,ALL,0

ALLSEL
NSEL,S,LOC,X,length
CP,1,UZ,ALL

ALLSEL
F,4555,FZ,width
EPLOT

TREF,0
TUNIF,50

ALLSEL
/SOLU
SOLVE
FINISH
```

C.2 Ansys 10 Batch Code for Circular Tube

```
/FILNAM, Composite Tube
/TITLE, Composite Tube

/UNITS,BIN
/PREP7

LOCAL,11,CYLIN,0,0,0,0,90,90

!~~~~~~~~~~~~~~~~~~~~~~~~~~~~~~~~~~~~~~~~~~~~~~~~~~~~~~~~~~~~~~~~~~~~
!Define the input varianles
!~~~~~~~~~~~~~~~~~~~~~~~~~~~~~~~~~~~~~~~~~~~~~~~~~~~~~~~~~~~~~~~~~~~~

tply=0.005
r=1+tply*8
length=10

!~~~~~~~~~~~~~~~~~~~~~~~~~~~~~~~~~~~~~~~~~~~~~~~~~~~~~~~~~~~~~~~~~~~~
!Define Material Properties
!~~~~~~~~~~~~~~~~~~~~~~~~~~~~~~~~~~~~~~~~~~~~~~~~~~~~~~~~~~~~~~~~~~~~

!Carbon/Epoxy AS4/3501-6
MP,EX,1,21.3E6
MP,EY,1,1.5E6
MP,EZ,1,1.5E6
MP,PRXY,1,0.27
MP,PRXZ,1,0.27
MP,PRYZ,1,0.27
MP,GXY,1,1.0E6
MP,GXZ,1,1.0E6
MP,GYZ,1,1.0E6
MP,ALPX,1,-0.5E-6
MP,ALPY,1,15E-6
MP,ALPZ,1,15E-6

!~~~~~~~~~~~~~~~~~~~~~~~~~~~~~~~~~~~~~~~~~~~~~~~~~~~~~~~~~~~~~~~~~~~~
!Define Element Type and Real Constants
!~~~~~~~~~~~~~~~~~~~~~~~~~~~~~~~~~~~~~~~~~~~~~~~~~~~~~~~~~~~~~~~~~~~~

ET,1,SOLID46

R,1
```

```
RMODIF,1,1,1,0,0,0,0
RMODIF,1,7,0
RMODIF,1,13,1,45,tply

R,2
RMODIF,2,1,1,0,0,0,0
RMODIF,2,7,0
RMODIF,2,13,1,-45,tply

R,3
RMODIF,3,1,1,0,0,0,0
RMODIF,3,7,0
RMODIF,3,13,1,90,tply

R,4
RMODIF,4,1,1,0,0,0,0
RMODIF,4,7,0
RMODIF,4,13,1,0,tply

R,5
RMODIF,5,1,1,0,0,0,0
RMODIF,5,7,0
RMODIF,5,13,1,90,tply

R,6
RMODIF,6,1,1,0,0,0,0
RMODIF,6,7,0
RMODIF,6,13,1,0,tply

R,7
RMODIF,7,1,1,0,0,0,0
RMODIF,7,7,0
RMODIF,7,13,1,45,tply

R,8
RMODIF,8,1,1,0,0,0,0
RMODIF,8,7,0
RMODIF,8,13,1,-45,tply

R,9
RMODIF,9,1,1,0,0,0,0
RMODIF,9,7,0
RMODIF,9,13,1,-45,tply
```

```
R,10
RMODIF,10,1,1,0,0,0,0
RMODIF,10,7,0
RMODIF,10,13,1,45,tply

R,11
RMODIF,11,1,1,0,0,0,0
RMODIF,11,7,0
RMODIF,11,13,1,0,tply

R,12
RMODIF,12,1,1,0,0,0,0
RMODIF,12,7,0
RMODIF,12,13,1,90,tply

R,13
RMODIF,13,1,1,0,0,0,0
RMODIF,13,7,0
RMODIF,13,13,1,0,tply

R,14
RMODIF,14,1,1,0,0,0,0
RMODIF,14,7,0
RMODIF,14,13,1,90,tply

R,15
RMODIF,15,1,1,0,0,0,0
RMODIF,15,7,0
RMODIF,15,13,1,-45,tply

R,16
RMODIF,16,1,1,0,0,0,0
RMODIF,16,7,0
RMODIF,16,13,1,45,tply

!~~~~~~~~~~~~~~~~~~~~~~~~~~~~~~~~~~~~~~~~~~~~~~~~~~~~~~~~~~~~~~~~~~~~~~~~~~~
!Define the Geometry of the Beam
!~~~~~~~~~~~~~~~~~~~~~~~~~~~~~~~~~~~~~~~~~~~~~~~~~~~~~~~~~~~~~~~~~~~~~~~~~~~

CSYS,11

*DO,I,1,16,1
K,1+4*(I-1),r-tply*(I-1),0,0
K,2+4*(I-1),r-tply*(I-1),90,0
```

```
K,3+4*(I-1),r-tply*(I-1),180,0
K,4+4*(I-1),r-tply*(I-1),270,0
K,65+4*(I-1),r-tply*(I-1),0,length
K,66+4*(I-1),r-tply*(I-1),90,length
K,67+4*(I-1),r-tply*(I-1),180,length
K,68+4*(I-1),r-tply*(I-1),270,length
L,1+4*(I-1),2+4*(I-1)
L,2+4*(I-1),3+4*(I-1)
L,3+4*(I-1),4+4*(I-1)
L,4+4*(I-1),1+4*(I-1)
L,65+4*(I-1),66+4*(I-1)
L,66+4*(I-1),67+4*(I-1)
L,67+4*(I-1),68+4*(I-1)
L,68+4*(I-1),65+4*(I-1)
L,1+4*(I-1),65+4*(I-1)
L,2+4*(I-1),66+4*(I-1)
L,3+4*(I-1),67+4*(I-1)
L,4+4*(I-1),68+4*(I-1)
*ENDDO

*DO,J,1,16,1
AL,1+12*(J-1),9+12*(J-1),5+12*(J-1),10+12*(J-1)
AL,2+12*(J-1),10+12*(J-1),6+12*(J-1),11+12*(J-1)
AL,3+12*(J-1),11+12*(J-1),7+12*(J-1),12+12*(J-1)
AL,4+12*(J-1),12+12*(J-1),8+12*(J-1),9+12*(J-1)
*ENDDO

*DO,K,1,64,1
VOFFST,K,-tply
*ENDDO

NUMMRG,KP,1.0e-4

!~~~~~~~~~~~~~~~~~~~~~~~~~~~~~~~~~~~~~~~~~~~~~~~~~~~~~~~~~~~~~~~~~~~~~~~~
!Define number of the Element on Each Line
!~~~~~~~~~~~~~~~~~~~~~~~~~~~~~~~~~~~~~~~~~~~~~~~~~~~~~~~~~~~~~~~~~~~~~~~~

LSEL,S,,,1,8,1
*DO,L,1,15,1
LSEL,A,,,1+12*L,8+12*L,1
*ENDDO
lplot
LESIZE,ALL,,,9
```

```
LSEL,S,,,9,12,1
*DO,M,1,15,1
LSEL,A,,,9+12*M,12+12*M,1
*ENDDO
lplot
LESIZE,ALL,,,20

CSYS,0

LSEL,S,LOC,Z,0
LSEL,R,LOC,X,0
LESIZE,ALL,,,1

LSEL,S,LOC,Y,0
LSEL,R,LOC,X,0
LESIZE,ALL,,,1

LSEL,S,LOC,Z,0
LSEL,R,LOC,X,length
LESIZE,ALL,,,1

LSEL,S,LOC,Y,0
LSEL,R,LOC,X,length
LESIZE,ALL,,,1

!~~~~~~~~~~~~~~~~~~~~~~~~~~~~~~~~~~~~~~~~~~~~~~~~~~~~~~~~~~~~~~~~~~~~~~~~
!Mesh the Volumes
!~~~~~~~~~~~~~~~~~~~~~~~~~~~~~~~~~~~~~~~~~~~~~~~~~~~~~~~~~~~~~~~~~~~~~~~~

ALLSEL
*DO,N,1,16,1
TYPE,1,
ESYS,0
MAT,1,
REAL,N
VMESH,1+4*(N-1),4+4*(N-1),1
*ENDDO
EPLOT

!~~~~~~~~~~~~~~~~~~~~~~~~~~~~~~~~~~~~~~~~~~~~~~~~~~~~~~~~~~~~~~~~~~~~~~~~
!Merge All Coincident Nedes,Elements, and Key points
!~~~~~~~~~~~~~~~~~~~~~~~~~~~~~~~~~~~~~~~~~~~~~~~~~~~~~~~~~~~~~~~~~~~~~~~~
```

```
ALLSEL
NUMMRG,NODE,1.0e-4
NUMMRG,ELEM,1.0e-4
NUMMRG,KP,1.0e-4
EPLOT

!~~~~~~~~~~~~~~~~~~~~~~~~~~~~~~~~~~~~~~~~~~~~~~~~~~~~~~~~~~~~~~~~~~~~~~~~
!Apply Constraints, Load, and Temperature Change
!~~~~~~~~~~~~~~~~~~~~~~~~~~~~~~~~~~~~~~~~~~~~~~~~~~~~~~~~~~~~~~~~~~~~~~~~

NSEL,S,LOC,X,0
D,ALL,ALL,0

NSEL,S,LOC,X,length
CP,1,UZ,ALL
F,11,FZ,-10

TREF,0
TUNIF,50

EPLOT

ALLSEL
/SOLU
SOLVE
FINISH
```

REFERENCES

1. Chan, W.S. and Demirhan, K.C., "A Simple Closed-Form Solution of Bending Stiffness for Laminated Composite Tube", Journal of Reinforced Plastics and Composites, v 19, No. 04, 2000, p 278-291.

2. Lin, C.Y. and Chan, W.S., "A Simple Analytical Method for Analyzing Laminated Composite Elliptical Tubes", Proceedings of 17th Technical Conference, American Society of Composites, Oct. 2002.

3. Roa, C.S., "Analysis of Tapered Laminated Composite Tubes under Tension and Torsion", Master's Thesis, University of Texas at Arlington, May 2007.

4. Sims, D.F. and Wilson, H.E., "Distribution of Shearing Stresses in a Composite Beam under Transverse Loading", Composites, July 1978, p 185-191.

5. Syed, K.A. and Chan, W.S., "Analysis of Hat-Sectioned Reinforced Composite Beams", Proceedings of American Society of Composites, Sept. 2006.

6 Boley, B.A. and Weiner, J.H., 1997, *Theory of Thermal Stresses*, Dover Publications, INC., Mineola, NY.

7. Naidu, N.V.S. and Sinha, P.K., "Nonlinear Finite Element Analysis of Laminated Composite Shells in Hygrothermal Environment", Composites Structures, v 69, 2005, p 387-395.

8. Seibi, A.C. and Amatcau, M.F., "Finite Element Modeling and Optimization for Controlling the Residual Thermal Stresses of Laminated Composite Tubes", Composite Structures, v 41, 1998, p 151-157.

9. Shariyat, M., "Thermal Buckling Analysis of Rectangular Composite Plate with Temperature-Dependent Properties based on a layerwise theory", Thin-Walled Structures, v 45, 2007, p 439-452.

10. Kim, B.-S., Kim, T.-W., Byun, J.-H., and Lee, W.-I., "Stress Analysis of Composite/Ceramic Tube Subjected to Shrink Fit, Internal Pressure and Temperature Differences." Key Engineering Materials, v 137, 1998, p 32-39.

11. Khdeir, A. A., "Thermal Buckling of Cross-Ply Laminated Composite Beam." ACTA Mechanica, v 149, n 1-4, 2001, p 201-213.

12. Syed, K.A., Su, C.W., and Chan, W.S., "Analysis of Fiber Reinforced Composite Beams under Temperature Environment", Proceedings of the Seventh International Congress on Thermal Stresses, Taipei, Taiwan, 2007.

13. Gay, P. and Hoa, S.V., 2007, *Composite Material Design and Applications second edition*, CRC Press.

14. Tuttle, M.E., Chapter 5 and 6 in *Structural Analysis of Polymeric Composite Materials*, Marcel Dekker, INC., New York, NY.

15 Daniel, I.M. and Ishai, O., 2006, Chapter 7 and 8 in *Engineering Mechanics of Composite Material second edition*, Oxford University Press, INC., New York, NY.

BIOGRAPHICAL INFORMATION

Chia-Wei Su received his B.S. degree in Mechanical Engineering from Mingchi University of Technology, Taipei, Taiwan in 2002. He started his master's program in Mechanical Engineering at the University of Texas at Arlington in August 2005. His research interests include structural analysis, finite element analysis, fatigue and fracture mechanics, and composite structures.

Chia-Wei Su received his master's degree in mechanical engineering from the University of Texas at Arlington in December 2007.